

This is an Open Access document downloaded from ORCA, Cardiff University's institutional repository: <https://orca.cardiff.ac.uk/id/eprint/91322/>

This is the author's version of a work that was submitted to / accepted for publication.

Citation for final published version:

Sanislav, I. V., Brayshaw, M., Kolling, S. L., Dirks, P. H. G. M., Cook, Y. A. and Blenkinsop, Thomas 2017. The structural history and mineralization controls of the world-class Geita Hill gold deposit, Geita Greenstone Belt, Tanzania. *Mineralium Deposita* 52 (2) , pp. 257-279. 10.1007/s00126-016-0660-1

Publishers page: <http://dx.doi.org/10.1007/s00126-016-0660-1>

Please note:

Changes made as a result of publishing processes such as copy-editing, formatting and page numbers may not be reflected in this version. For the definitive version of this publication, please refer to the published source. You are advised to consult the publisher's version if you wish to cite this paper.

This version is being made available in accordance with publisher policies. See <http://orca.cf.ac.uk/policies.html> for usage policies. Copyright and moral rights for publications made available in ORCA are retained by the copyright holders.



**The structural history and mineralization controls on the world-class  
Geita Hill gold deposit, Geita Greenstone Belt, Tanzania**

I. V. Sanislav<sup>a\*</sup>, M. Brayshaw<sup>b</sup>, S. L. Kolling<sup>b</sup>, P. H. G. M. Dirks<sup>a</sup>, Y. A. Cook<sup>a</sup>, T. G. Blenkinsop<sup>c</sup>

<sup>a</sup> Economic Geology Research Centre (EGRU) and Department of Earth and Oceans, James Cook University, Townsville, 4011, QLD, Australia; e-mail: [ioan.sanislav@jcu.edu.au](mailto:ioan.sanislav@jcu.edu.au); phone: (+61) 07 4781 3293; fax: (+61) 07 4781 5581

<sup>b</sup> Geita Gold Mine, Geita, P.O. Box 532, Geita Region, Tanzania

<sup>c</sup> School of Earth & Ocean Sciences, Cardiff University, Cardiff CF10 3AT, United Kingdom

## Abstract

The Geita Hill gold deposit is located in the Archean Geita Greenstone Belt and is one of the largest and longest operating gold deposits in East Africa. The Geita Greenstone Belt experienced a complex deformation and intrusive history that is well illustrated and preserved in and around the Geita Hill gold deposit. Deformation involved early stages of ductile shearing and folding ( $D_1$  to  $D_5$ ), during which episodic emplacement of large diorite intrusive complexes, sills and dykes occurred. These ductile deformation phases were followed by the development of brittle-ductile shear zones and faults ( $D_6$  to  $D_8$ ). The last stages of deformation were accompanied by voluminous felsic magmatism involving the intrusion of felsic porphyry dykes, within the greenstone belt and the emplacement of large granitoid bodies around the greenstone belt margins. Early, folded lamprophyre dykes, and later lamprophyre dykes, crosscutting the folded dykes are common, although volumetrically insignificant. The gold deposit formed late during the tectonic history of the greenstone belt, post-dating ductile deformation and synchronous with the development of brittle-ductile shear zones that overprinted earlier structural elements. The main mineralizing process involved sulphide replacement of magnetite-rich layers in ironstone and locally the replacement of ferromagnesian phases and magnetite in the diorite intrusions. The intersection between the brittle-ductile ( $D_6$ ) Geita Hill Shear Zone and different structural elements of ductile origin (e.g. fold hinges), and the contact between banded ironstone and folded diorite dykes and sills provided the optimal sites for gold mineralization.

Keywords: Archean; Geita Hill; gold deposits; structural controls; Tanzania

## 1. Introduction

Archean granite-greenstone terrains are one of the most important sources of gold worldwide (e.g. Goldfarb et al. 2010) and have been the subject of numerous geological studies (e.g. Groves et al. 1998; Goldfarb et al. 2001; Groves et al. 2003; Blenkinsop 2004; Bierlein et al. 2009; Dirks et al. 2009; Blewett et al. 2010; Dirks et al. 2013). Most Archean gold deposits show a strong structural control and late-tectonic, brittle-ductile shear zones have proven to be particularly fertile (e.g. Hageman et al. 1992; Groves et al. 1998; Miller et al. 2010; Dirks et al. 2013). Regionally, gold deposits are generally linked to first order shear zones, but at the deposit-scale the controlling structures are second or third order structures (Cassidy et al. 1998; Blenkinsop et al. 2000; Weinberg and van der Borgh 2008; Dirks et al. 2013).

Many studies show that structures that control mineralization are related to the late-tectonic reactivation of earlier shear zones (Witt and Vanderhor 1998; Dirks et al. 2009). The formational origin of the mineralised structures can be controversial. They are commonly interpreted as secondary structures to major shear zones, mostly thrusts or strike-slip zones (e.g. Colvine et al. 1988; Robert et al. 1991; Leclair et al. 1993), but alternatively controlling structures are later faults that truncate the shear zones (Dirks et al. 2009, 2013; Tripp and Vearcombe 2004). The importance of identifying the nature of the mineralised structures has been highlighted in numerous studies (e.g. Stokes et al. 1990; Miller et al. 2010; Blewett et al. 2010) and understanding such structures is critical for regional exploration targeting.

The Archean Tanzanian Craton hosts a number of world-class gold deposits (e.g. Geita, Bulyanhulu, North Mara, Buzwagi) making it a major gold producing region in Africa. Gold mineralization in Tanzania is generally associated with Neoarchean granite-greenstone terrains (Kabete et al. 2012), which broadly trend E-W, and have been subdivided into six major greenstone belts (Borg et al. 1990): the Sukumaland, Nzega, Iramba-Sekenke, Shynianga-Malita, Kilimafedha and North Mara greenstone belts (Fig. 1). Of these, the

Sukumaland Greenstone Belt has produced the most gold, hosting the largest and highest number of gold deposits. The Sukumaland Greenstone Belt comprises partly connected greenstone fragments (e.g. Borg and Shackleton 1997). A larger one of these fragments in the north of the belt has been reclassified as the Geita greenstone Belt (Sanislav et al. 2014).

The Geita Hill gold deposit is located within the Geita Greenstone Belt (Sanislav et al. 2014), which also hosts a number of other major deposits (e.g. Lone Cone, Nyankanga, Area3, Kukuluma, Matandani, Chipaka, Pit 30, Ridge 8, Star & Comet and Roberts – all of which with resources of >100,000 oz; Fig. 1). The greenstone belt currently produces ~500,000 oz of gold per year from three active open pit operations.

The Geita Hill gold deposit has been one of the longest and largest operating gold mine in East Africa with gold production starting in 1936 (Borg 1994). Previous studies on gold deposits within the Tanzania Craton have focused on their regional distribution (Gabert 1990; Kuehn et al. 1990; Kabete et al. 2012), genesis and timing (Borg et al. 1990; Borg 1994; Walraven et al. 1994; Borg and Krogh 1999; Borg and Rittenauer 2000), and associated igneous rocks and geochemistry (Borg 1994; Cloutier et al. 2005; Kwelwa et al. 2013), and less on their structural control (Borg 1994; Vos et al. 2009; Sanislav et al., 2015). This paper presents a detailed structural analysis for the rocks around Geita Hill that host the world-class Geita Hill Gold deposit and the nearby Lone Cone and Nyankanga deposits (Fig. 2). This area is heavily mined and provides excellent outcrop in a number of open pits. It is well-suited to develop a deformational framework in relation to mineralization and the complex intrusive history that places important constraints on the tectonic evolution of this part of the Tanzania Craton. The detailed structural history compiled in this study (Table 1) can be used for comparative purposes across the greenstone belt, and to test the validity of existing stratigraphic and tectonic models.

## 2. Geological setting

The stratigraphy of the Tanzania Craton has been subdivided into three main units. The oldest unit is the Dodoman Supergroup, which consists of high-grade mafic and felsic granulite with subordinate lower-grade schist and thin slivers of greenstone (Kabete et al. 2012). The Nyanzian Supergroup has been placed stratigraphically above the Dodoman Supergroup (e.g. Quennel et al. 1956; Gabert 1990) and comprises the Lower Nyanzian, dominated by mafic volcanic units (amphibolite, pillow basalt, minor gabbro) overlain by the Upper Nyanzian, dominated by felsic volcanic and pyroclastic units inter-bedded with banded ironstone, volcanoclastic sequences and immature turbiditic sediment (Kuehn et al. 1990; Borg 1992; Borg and Shackelton 1997; Borg and Krogh 1999). The Nyanzian Supergroup is unconformably overlain by the Kavirondian Supergroup, which consists mainly of coarse-grained conglomerate, grit and quartzite. It was interpreted to be the equivalent to the molasse facies within greenstone belts (e.g. Gabert 1990).

The Sukumaland Greenstone Belt has been described as an arcuate-shaped belt in which intrusions of syn- to post-tectonic granitoid divide the belt into an inner arc dominated by mafic volcanic rocks and an outer arc dominated by banded ironstone, felsic tuff and volcanoclastic sediment (Borg et al. 1990; Borg 1994). This subdivision may be too simplistic as indicated by the occurrence of abundant mafic units in the outer arc and abundant sediment and felsic volcanic intercalations in the inner arc (e.g. Cloutier et al. 2005; Many and Maboko 2008).

The Geita Greenstone Belt (GGB, Fig. 2) forms an E-W trending (80 x 25km) portion of greenstone that constitutes most of the northern part of the outer arc of the Sukumaland greenstone belt (Borg et al. 1990). Along its southern margin, the GGB is in contact with gneiss and mylonitic granitoid along a steeply dipping, broadly E-W trending shear zone. The northern, eastern and western parts of the greenstone belt have been intruded by late syn- to

post-tectonic granitoid plutons and stocks with ages between 2660 and 2620 Ma (Sanislav et al. 2014). The southern part of the GGB contains a mafic unit with amphibolite, variably deformed pillow lava and minor gabbro. Geochemistry and whole rock Sm-Nd ages for these rocks indicate a MORB-like affinity and model ages of ca. 2823 Ma (Manyà and Maboko 2008). The remainder of the greenstone belt is dominated by banded ironstone intercalated and overlain by turbiditic metasedimentary units (ranging from mudstone to rare conglomerate) with volcanoclastic beds, and intruded by diorite dykes and sills, and late granitoids. Borg and Krogh (1999) dated a trachyandesite sub-parallel to bedding (and interpreted as an extrusive unit) from Geita Hill, at  $2699 \pm 9$  Ma, which they interpreted as an estimate for the depositional age of the sedimentary sequence in the area; although the development of the open pit suggests that the unit they dated was probably a fine-grained dioritic sill and not an extrusive unit. NE-striking, Neoproterozoic dolerite dykes cross-cut the GGB.

## **2.1 Exploration, mining and regional geology around Geita Hill Gold Mine**

The Geita Hill gold deposit lies within a 6-7 km long, ENE-WSW trending mineralized zone within the nose of a regional scale fold structure that closes to the SE (Fig. 2). This WSW-trending, Geita mineralized zone has accounted for the vast majority of gold produced in the GGB, and also includes the Lone Cone and Nyankanga deposits to the WSW of Geita Hill. Gold mineralization was first discovered in the Geita district in 1898 by a German prospector (e.g. Cowley, 2001). A regional survey by a Kenyan company, Saragura Prospecting Syndicate, followed in 1930. A mine was developed in 1934, and between 1936 and closure in 1966, the Geita mine was the largest gold mine in East Africa, producing a million ounces from underground operations. Mining took place on 9 levels, each between 400 and 800 meters long and 45 to 50 meters apart. Exploration in the GGB was resumed in the mid-1990's and mining at Geita Hill recommenced as an open pit operation in 2002.

Carter (1959) described the mineralization at Geita Hill as widespread, disseminated sulphide replacement (mainly pyrite and pyrrhotite) in fractured zones in ironstone with quartz-calcite stringers and veins accompanying mineralization to give rise to large, low-grade, stockwork-type ore bodies, with mining controlled by assay limits. Borg (1994) and Borg and Rittenauer (2000) identified that gold is related to late stage euhedral pyrite that overgrows the structural fabric suggesting that gold deposition post-dated deformation.

The stratigraphic units hosting the Geita Hill deposit (Figs. 3a and b) and the nearby Lone Cone and Nyankanga deposits consist of a thick pile of sandstone, siltstone and shale beds that were deposited at ~2700 Ma (Borg and Krogh 1999; Chamberlain and Tosdal 2007; Sanislav et al., 2015) and metamorphosed to upper greenschist facies (e.g. Borg, 1994). Clastic sediments are interbedded with black shale, thought to be deposited in a volcanogenic, oxygen-poor environment. Apart from the black shale units all sedimentary units are interpreted as turbidite beds, deposited in a prograding submarine deltaic or delta-fan environment (Krapez et al. 2003; Sanislav et al., 2015).

The turbidite sequence generally consists of immature, chlorite-plagioclase-bearing metasedimentary rocks originally derived from an andesite-rich source (Borg 1994). The sequence contains several horizons of massive, graded beds of coarse-grained, quartz-feldspar-rich sandstone horizons that contain pebbles up to 15cm in size, representing high-energy event horizons derived most probably from a proximal rhyolitic to dacitic source. The stratigraphically lowermost pebble-rich, quartz-sandstone bed is several metres thick and forms a distinct marker horizon within the sedimentary pile.

Fine-grained magnetite-rich siltstone, shale and chert (Fig. 4a and 4b) is common throughout the turbidite sequence. Magnetite banding is para-concordant to highly discordant to bedding, and commonly anastomosing. The beds are extensively silicified and epigenetic pyrite is common, especially near and within ore zones (e.g. Borg and Rittenauer 2000).



Layers and lenses of bedded chert, up to 50 cm thick, are common in association with fine-grained, magnetite-rich layers, and are interpreted to result from early-diagenetic replacement of sediments near the sea floor during periods of non-deposition (Krapez et al. 2003). Chert was deposited near the stratigraphic top of fining upward cycles, indicating waning pulses of clastic deposition or periods of tectonic inactivity. Chert beds are less common in coarser-grained turbiditic sandstone units.

Silicification is wide-spread throughout the turbidite sequence, rendering the unit chert-like and flinty. Because of silicification, the well-bedded nature of the sequence, and the presence of extensive, near-concordant magnetite alteration in association with chert beds, this unit is generally referred to by the mine as BIF, and the Geita Gold Mine is, therefore, commonly classified as a BIF-hosted, rather than a clastic sediment-hosted deposit (e.g. Borg et al. 1990; Gabert 1990; Kuehn et al. 1990; Borg 1994; Kabete et al. 2012). Because of early diagenetic alteration and superposed deformation this unit resembles in many places highly strained amorphous siliceous alteration (cherty), but since we were unable to definitely test this hypothesis we will use the descriptive names chert and ironstones.

The sedimentary pile hosts numerous intrusions with a wide variety of compositions and textures. Variably foliated sills, dykes and stocks (Fig. 4c, d) with dioritic composition are common throughout the Geita Hill area, and merge into a larger diorite body at depth, which makes up the greater part of the pit at the Nyankanga deposit, forming the Nyankanga Intrusive Complex (Sanislav et al. 2015). Field evidence, such as dykes radiating from the Nyankanga Intrusive Complex, suggests that the Nyankanga Intrusive Complex extends beneath the supracrustal package hosting the Geita deposit (Fig. 5). Diorite intrusions (Fig. 4c, d) have a dark groundmass of altered feldspar and mafic minerals with phenocrysts of plagioclase and/or hornblende. Fine-grained quartz forms <5% of total modal mineralogy.

Primary phenocrysts of hornblende can be abundant; they are green to dark brown with an acicular habit, and are usually replaced by biotite or actinolite-carbonate. Plagioclase phenocrysts vary in size and distribution, but can be up to 1 cm in length, and are commonly replaced by fine-grained sericite. Biotite phenocrysts are rare and where present make up < 5% of the total modal mineralogy. The diorite in Nyankanga pit has been dated at  $2698 \pm 14$  Ma (U-Pb zircon, Chamberlain and Tosdal 2007). A date of  $2699 \pm 9$  Ma reported by Borg (1994) for an extrusive trachyandesite unit, was probably derived from a diorite sill, rather than a lava flow, which have not been observed in the pit, and is consistent with the age of the diorite intrusion. In this context it is important to note that the dates reported by Borg (1994) were based on sampling of poorly preserved and spatially limited underground exposures of the abandoned Geita Mine.

The sedimentary pile is also cut by late-tectonic quartz-feldspar porphyry and quartz porphyry dykes of granodioritic composition (Fig. 4e), dated at  $2695 \pm 18$  Ma and  $2689 \pm 11$  Ma, respectively (U-Pb zircon; Chamberlain and Tosdal 2007). Quartz-feldspar porphyries and quartz porphyries are rare and usually occur as cross-cutting dykes. They have a fine-grained groundmass, are light to medium grey in colour, with a weak to moderate porphyritic texture. Plagioclase phenocrysts form the main porphyritic phase, but smaller porphyry bodies with rounded quartz augen and minor hornblende are also present.

Two generations of biotite-rich lamprophyre (Fig. 4f) dykes transect the sedimentary pile: early syn-tectonic lamprophyre dykes dated in Nyankanga pit at  $2686 \pm 13$  Ma (U-Pb-zircon, Chamberlain and Tosdal 2007) and late tectonic lamprophyre dykes sampled in the Geita underground mine, dated at  $2644 \pm 3$  Ma (U-Pb zircon; Borg and Krogh 1999). The early generation of lamprophyre dykes is folded and strongly sheared and altered, with most mafic minerals replaced by fine-grained biotite and carbonate. The second generation of

lamprophyre dykes are fresh with shearing developed only along dyke margins, and they crosscut the folded sequence.

### **3. The history of deformation and intrusion at Geita Hill**

Little detailed structural work from the GGB has been published in spite of the fact that the gold mineralization is generally considered to be structurally controlled, and to represent a typical orogenic gold deposit (e.g. Goldfarb et al. 2001; Bierlein et al. 2009). The most detailed work on Geita Hill gold deposit comes from Borg (1994), which highlights the epigenetic nature of the gold mineralization. Early survey reports (Horne 1959; Carter 1959) provide useful observations of mineralized structures at the time the mine was developed as an underground mine, and old mine plans (Fig. 6; Borg 1994) provide further constraints on structural relationships.

This paper proposes a deformation scheme for the structures encountered in the Geita Hill deposit and adjacent areas, and their association with intrusive phases and mineralization, based on mapped overprinting relationships and available age data (Table 1; Chamberlain and Tosdal 2007; Sanislav et al. 2014, 2015).

All the data presented in this study is based on mapping and structural interpretations from the Geita Hill open pit and surrounding outcrops. All planar structural data is reported as dip direction and dip. Data was collected from mapping, core logging and underground mine plans held in the Geita Gold Mine database. The high grade ore lenses along the Geita Hill Shear Zone were defined using grade control drilling and drilling that targeted the underground extensions of the mineralization. The gold mineralization envelope referred to in this paper is based on a cut-off grade of 0.5 g/t. The relationship between the structures, alteration and mineralization was assessed, based on detailed pit wall mapping of the mineralized zones. Alteration and structural domains were identified on each observation

point and representative samples were assayed for gold with results superimposed on geological and structural maps.

### **3.1 Deformation sequence in and around the Geita Hill gold deposit**

Deformation structures at Geita Hill fall into two broad groups: an early group of deformation structures resulting from folding and shearing events, which occurred when the rocks were fully ductile ( $D_1$ - $D_5$ ), and a later group of structures formed during brittle-ductile shearing and faulting events ( $D_6$ - $D_8$ ), which are more localised and associated with the main phase of mineralization. Deformation events were accompanied by a wide range of felsic and intermediate intrusions, which will be described separately. The events have been summarised in Table 1.

#### **3.1.1 $S_0$ and $D_1$ layer-parallel shearing events**

Evidence for the earliest tectonic deformation events, grouped as  $D_1$ , is contained within the compositional banding of the well-layered, silicified turbidite sequence or bedded ironstone units. The sequence contains para-concordant and anastomosing magnetite banding, and associated silicification, including chert banding, which overprint sedimentary bedding to result in a well-layered sequence of rocks, which, in places, reflects primary sedimentary layering, and elsewhere reflects a more complex compositional banding of unknown origin, which we refer to as  $S_0$ .  $D_1$  deformation structures are best preserved in ~ 20 cm thick layers of fine, grey-green chert that truncate  $S_0$  at a low angle ( $<5^\circ$ ) to primary bedding, and that are exposed along the road cutting mapped in Figure 7. Internal and restricted to the chert beds are several phases of highly non-cylindrical, disharmonic, flow-folds, and the fabric has an ultra-fine-grained texture. These internally deformed chert units

have been interpreted as an early phase of near-layer-parallel shear zones. No reliable shear sense could be determined.

The chert layers, as well as other laminated chert horizons within  $S_0$ , were boudinaged prior to later folding events. The extent of boudinaging of  $S_0$  varies, but in several places discrete, thin (5cm) chert beds have been stretched >300% (Fig. 8a), indicating that zones of high extensional strain are contained within  $S_0$ . We refer to the fabric in these highly-strained areas as a composite  $S_0/S_1$ , transposition fabric to reflect the early strain history, in which  $S_0$  and  $S_1$  are parallel to each other. Isolated boudins locally contain isoclinal fold-hinges ( $F_1$ -folds), mostly with a steep westerly plunge and S-like asymmetry ( $\sim 250/65$  based on 7 measurements; Fig. 8b). Zones with high-strain  $S_0/S_1$  fabrics preserve a  $D_1$  mineral stretching lineation defined by elongated quartz on  $S_0/S_1$  planes that plunges W at a shallow angle ( $\sim 230/12$  based on 4 measurements along the road cutting mapped in Figure 7). This lineation and the asymmetry of  $F_1$  folds suggest that  $D_1$  extensional strain in the area of Figure 7, originated from sinistral movement along  $S_0/S_1$  in the current orientation of  $S_0/S_1$ .

Figure 9a shows a stereoplot of poles to  $S_0/S_1$  for the Geita Hill deposit and the surrounding metasediments. The bedding orientation, although variable, shows a consistent NE trend and dips moderately NW (averaging at  $301/40$ ). The spread of data arises from later folding detailed below.

### 3.1.2 $D_2$ - second phase of regional dis-harmonic, non-cylindrical folding

$D_2$  events are characterised by the pervasive development of cm- to m- scale (rarely up hundred metres scale), highly non-cylindrical folds with a large range of geometries and a wide dispersion in fold axes orientations. Larger scale folds may be present, but are hard to recognise owing to later deformation overprints.  $D_2$  folds are generally plunging-inclined,

with moderately NW dipping axial planes, and vary from near isoclinal, to open, near-cylindrical, parallel folds, box folds and chevron-like folds, with fold geometries partly dictated by lithology and the strength of the underlying  $S_0/S_1$  layering.

Around Geita Hill (Figs. 7 and 8),  $D_2$  folds are common and  $F_2$  fold axis orientations are homogeneously distributed along a great circle (Fig. 7; 325/64; Bingham solution eigenvalues  $ev_1$ : 242/14;  $ev_2$ : 358/60 and  $ev_3$ : 145/26, with eigenvalues of 0.5016, 0.4735 and 0.0250, respectively) reflecting the non-cylindrical nature of the  $F_2$  folds, some of which assume sheath-like geometries (Fig. 8c). Within chert-magnetite-rich units, axial planar,  $S_2$  fabrics are weak to absent, however, within inter-bedded shale horizons  $S_2$  is well developed as a penetrative, moderately NW to WNW dipping, slaty cleavage.

Within the Geita Hill deposit,  $F_2$  folds are common, and plunge predominantly to the W to SW (Fig. 9b; between 230/30 and 290/70). The majority of the  $D_2$  folds have a z-vergence, possibly indicative of a large-scale, antiformal,  $D_2$  fold closure to the south of the deposit. Alternatively, there is a possibility of a “corridor” of S- and Z-folds transitioning to a high strain zone to the south where folds have been compressed and transposed parallel to bedding. Variations in fold axis orientations in part resulted from  $D_3$  fold overprints (Fig. 3b) described below.

### **3.1.3 $D_3$ - third phase of ductile folding**

$D_3$  events are characterised by widespread development of cm- to 100 m-scale folds with regular, near cylindrical geometries and relatively constant, NW-plunging fold axes (Fig. 9b).  $D_3$  folds overprint  $D_2$  structures, locally resulting in complex, m-scale, fold interference patterns that vary from type 2 to type 3 patterns (e.g. Forbes et al. 2004; Grasemann et al. 2004) depending on the non-cylindrical nature and orientation of the

underlying D<sub>2</sub> folds (see Fig. 8d). Fold interference also leads to dispersion of F<sub>3</sub> fold axes (Fig. 9b).

D<sub>3</sub> folds are generally plunging-inclined folds, with moderately NW dipping axial planes (Fig. 9c), and vary from closed to open, near-cylindrical, parallel folds, that locally assume crenulation-like geometries. Along the access ramp (Fig. 7), D<sub>3</sub> folds occur towards the north of the ramp as several, 20 m-scale, open plunging-inclined, S-folds, with extensive dm-scale crenulation folding along the hinge zones giving the folds a kink-like appearance. Within chert-magnetite-rich units, axial planar, S<sub>3</sub> fabrics have developed as a spaced fracture cleavage, and within inter-bedded shale horizons S<sub>3</sub> is well developed as a penetrative, moderately NW dipping, crenulation cleavage.

Within the Geita Hill gold deposit, F<sub>3</sub> fold axial planes dip moderately NW (Fig. 9c) and axes plunge moderately NW (~327/42; Fig. 9b). Unlike D<sub>2</sub> folds, D<sub>3</sub> folds display only S-asymmetry, reflecting the presence of 100-m scale, plunging-inclined, D<sub>3</sub> folds. A good example of a large-scale, closed (interlimb angle of ~65°) antiform-synform fold pair (with an overall S-asymmetry) was exposed in the open pit, where it coincided with the main ore zone, now removed by mining (Fig. 10). These D<sub>3</sub> folds affect sediments interlayered with 15-20 m-wide diorite sills, and plunge NNW (347/47), with an axial planar orientation of ~327/42 (i.e. sub-parallel to the average regional orientation of S<sub>0</sub>/S<sub>1</sub>, Fig. 9a). They occur within the centre of the ore zone (Fig. 3b), and are similar to a fold hinge described along the ore zone in the old underground mine (Carter 1959; Borg 1994).

#### **3.1.4 D<sub>4</sub>- upright open cylindrical folding**

In parts of the deposit (Fig. 8e), 50 m scale, gentle, plunging-upright folds occur, with near-vertical, NW trending, fold axial planes (215/90), and a NW plunge (~310/50). They

gently warp earlier folds and are locally associated with a spaced fracturing parallel to the fold axial plane. The regional extent of these folds is not clear.

### **3.1.5 D<sub>5</sub>-open sub-horizontal folding and thrusting**

The D<sub>2</sub>-D<sub>4</sub> fold interference patterns are overprinted by gentle, sub-horizontal to shallowly inclined horizontal folds that are apparent as undulations of the S<sub>0</sub>/S<sub>1</sub> bedding (Fig. 8f). In places the sub-horizontal folds are associated with a sub-horizontal, spaced fracturing, which may dip gently (<30 degrees) NW or SE, as well as shallowly NW or SE dipping fracture planes that record thrust movements of up to several meters. Some of the subhorizontal shear fractures associated with the D<sub>5</sub> folds locally displace the fracture cleavage associated with the D<sub>4</sub> folds indicating that D<sub>5</sub> postdates D<sub>4</sub>.

### **3.1.6 D<sub>6</sub>-Sinistral reverse shear zones and faults**

The folded sequence is cross-cut by several generations of brittle-ductile shear zones and faults. The earliest of these, referred to as D<sub>6</sub>, are networks of moderately to gently NW dipping, brittle-ductile shear zones that traverse the open pit, and have been linked to mineralization (cf. Borg, 1994). This system of D<sub>6</sub> shear zones is referred to here as the Geita Hill Shear Zone (GHSZ; Fig. 3a and b). They appear to be similar in nature and relative timing to the package of sinistral reverse shear zones associated with the main ore zone in the nearby Nyankanga deposit (Sanislav et al. 2015), except that they are located in the meta-sediments (Fig. 5). In the Geita Hill deposit, D<sub>6</sub> shear zones are preferentially developed in sedimentary lithotypes (Fig. 11a and b), whilst diorite bodies are less commonly sheared, with shear zones deflecting around intrusive margins ( Fig. 11c). D<sub>6</sub> shear zones cut across



the D<sub>2</sub> and D<sub>3</sub> folds (Fig. 3), and at the scale of the Geita Hill deposit no folding of D<sub>6</sub> shear zones by D<sub>4</sub> or D<sub>5</sub> folds has been observed. Therefore, these shear zones have been interpreted to post-date D<sub>1-5</sub> folding.

In the open pit at Geita Hill, individual D<sub>6</sub> shear zones are parallel to bedding at the mesoscopic scale (Fig. 11d and e). Where shear zones are well-developed, bedding is disrupted and chloritic shear bands have developed. Cataclasite is common where chert is dominant. Magnetite bands within the sedimentary rocks localize strain, resulting in entrainment of magnetite along the shear foliation. With increasing shear intensity, chlorite-magnetite-quartz segregations are apparent, and further attenuation yields chlorite-magnetite laminae with chert reduced to mm-sized fragments. Brittle deformation structures (veins, breccia zones) are more common in portions where the shear zone cuts across diorite units.

Based on historical underground mapping at Geita Hill (Fig. 6), a continuation of the GHSZ has been identified as a variably mineralized, NW-dipping, brittle-ductile deformation zone, which was delineated over a strike length of ~180m and interpreted as a reverse sinistral shear zone, based on drag folds and observed S-C structures. The shear zone is a moderately NW-dipping planar structure with a consistent down-dip orientation (305/52). It is associated with silicification and quartz veining (Carter 1959).

The GHSZ is exposed in the open pit across the central portion of the deposit where individual shears are sub-parallel to bedding. It becomes discontinuous and segmented towards the SW. This is illustrated in Figure 10, where the F<sub>3</sub> folds are cross-cut by a splay of fault segments, with minor offsets. However, at larger scale (Fig. 3) the GHSZ extends across the enveloping trace of bedding and it is sub-parallel to the axial trace of the large D<sub>3</sub> S-fold in the pit. Towards the SW, the GHSZ terminates into a splay of minor fractures and no major structure intersects the mineralized zones.

In the NE portion of the Geita Hill deposit, a prominent, D<sub>6</sub> brittle-ductile shear zone (316/60) characterized by a 15-30 cm wide, ferruginous and chloritic zone with fault gouge, has been mapped. This shear zone is an along-strike extension or en-echelon fault pair of the main GHSZ. Offset marker horizons (bedding planes and diorite dykes) along this fault suggest a sinistral reverse movement with a relatively small displacement (<5m). Slickenside surfaces (Fig. 3a) preserve an early generation of N to NW plunging lineations indicative of reverse sinistral movement overgrown by later generations of mainly W to WNW plunging lineations indicative of normal movement, possibly D<sub>7</sub> or D<sub>8</sub> in origin. The sub-horizontal lineations with a slight westerly plunge record a dextral-normal sense of movement, whereas sub-horizontal lineations with an easterly plunge record a sinistral-normal movement sense.

Within the general vicinity of the ore zone within the Geita Hill gold deposit, other NW dipping brittle-ductile shear zones with a sinistral reverse movement sense are exposed that are variably mineralized, and that preserve geometries and alteration zones similar to the Geita Hill Shear Zone (Fig. 11). These brittle-ductile shear zones dip moderately NW, mostly parallel to S<sub>0</sub>/S<sub>1</sub> layering (345/42-76). They are manifested as 70-80 cm wide, bleached and highly fractured zones with cataclasite and slickensided surfaces within a 2-3 m wide alteration halo, characterised by quartz veining and sulphide alteration. Internal duplexing and stepped slickensides (Fig. 8g) suggest sinistral to reverse sinistral movements along early slicken-line orientations (generally moderately to shallowly E-pitching). A second, younger set of W-pitching slickenlines (270/30), and S-C fabrics in cataclasite zones indicate a later (D<sub>7</sub>) phase of sinistral normal movement on the shear zones.

In summary, layer-parallel, moderately NW dipping brittle-ductile shear zones that are discontinuous along strike, occur across Geita Hill gold deposit, and some are locally mineralized (Fig. 12). These shears zones are characterised by a multi-staged deformation

history (D<sub>7</sub> or D<sub>8</sub> in timing) involving early sinistral reverse, and later normal movements, with only minor off-sets.

### 3.1.7 D<sub>7</sub> Sinistral and dextral shear zones

D<sub>6</sub> sinistral reverse shear zones were intruded by late-tectonic lamprophyre dykes (Figs. 6 and 9c). These biotite-rich dykes are common in and around the Geita Hill deposit (Fig. 7), where they are truncated, displaced, and reactivated along their margins by a set of steeply N dipping, brittle-ductile shear zones of D<sub>7</sub> origin. The D<sub>7</sub> shear zones parallel to lamprophyre dykes preserve shallowly east-plunging striations on slickensided fault planes that record dextral strike-slip displacements with a small normal component .

Within the deposit, D<sub>7</sub> brittle-ductile shear zones are common. Some occur as reactivations of D<sub>6</sub> shear zones and record both dextral and sinistral movements. D<sub>7</sub> dextral shear zones (Fig. 7) are generally steeply N-dipping (~010/70) and slickensided surfaces are consistent with dextral strike slip with a normal component of movement. The shear zones are up to 20 or 30 cm wide, and marked by gouge and chlorite alteration and S-C fabrics. Their relative timing can be ascertained from the fact that D<sub>7</sub> shear zones truncated, displaced, and reactivated the margins of late-tectonic, biotite-rich lamprophyre dykes, which intruded the D<sub>6</sub> shear zones.

The regional significance of the dextral and sinistral shear zones is unclear. However, NW trending dextral fault zones displaced the ore zone in the Nyankanga deposit, although no major dextral displacements of the ore zone are evident in the Geita Hill deposit.

### 3.1.8 D<sub>8</sub> fracture zones and normal faulting

D<sub>6</sub> slickensided shear zones preserve evidence of multiple stages of deformation, with the last stage being attributed to D<sub>8</sub> normal movement. The D<sub>8</sub> overprint of D<sub>6</sub> shear zones

can be recognized by the presence of slickensided fault surfaces that truncate D6-D7 fabrics and show a normal component of movement. Late-stage, normal faults (Fig. 8h) are common throughout the pit, and are mostly parallel to bedding (i.e. dip moderately NW). The normal faults are discrete narrow fractures that are locally slickensided with steeply NW-pitching lineations preserving a normal-sinistral movement sense. Rhomboidal quartz veins (Fig. 8h) are commonly developed at the extensional intersection of regular right-stepping fault segments.

## **3.2 Magmatic intrusions in relation to deformation**

Many different magmatic intrusions affect the sedimentary pile in the Geita Hill area, and were emplaced during and after the main ductile deformation events (Borg 1994). These intrusions fall into three groups: 1. Several generations of diorite intrusions with a wide range of textural variation, which can be subdivided into plagioclase diorite, hornblende diorite and fine-grained, equigranular diorite; 2. Lamprophyre dykes that are variably altered and deformed; and 3. Porphyritic granodiorite dykes that have been subdivided into feldspar porphyry, quartz porphyry and quartz-feldspar porphyry dykes. The relationship between these different intrusions and the different deformation events and mineralization are discussed below.

### **3.2.1 Diorite intrusions and deformation**

Mapping indicates that most diorite intrusions are sub-parallel to bedding; they locally truncate bedding planes, but mostly follow bedding trends or the axial planar surfaces of D<sub>2</sub> folds, resulting in a similar overall orientation of sills and dykes (Fig. 9d; ave. 316/40) as the bedding planes in the surrounding sediment (Fig. 9a).

Figure 7 shows that around the deposit, at least 4 types of diorite dykes and sills occur that vary in texture and grain size, and in the degree to which they have been foliated as a result of D<sub>2</sub> events. The diorite intrusions occur as 1-10 m wide sheets that intruded as sills, parallel to the compositional S<sub>0</sub>/S<sub>1</sub> bedding, or as dykes, truncating D<sub>2</sub> folded zones or parallel to the axial planar surfaces of D<sub>2</sub> folds. The sills and dykes are approximately parallel to each other and dip moderately NW (~320/60). Most are weakly foliated, with foliations parallel to the margins of the dykes and sills. This foliation is generally interpreted as S<sub>2</sub>, and the intensity of the foliation development can be tentatively used as a means to determine the relative age of intrusion in the absence of direct cross-cutting relationships (Fig. 3).

In the outcrops along the access ramp (Fig. 7), the most intensely foliated (and, therefore, presumed oldest) dyke is a microdiorite with distinct, mm-sized quartz augen and hornblende phenocrysts; the diorite truncates D<sub>2</sub> folds along their axial plane, and was probably emplaced during the late stages of D<sub>2</sub>. Several microdiorite dykes without visible quartz, also intrude parallel to S<sub>2</sub>, and are weakly foliated suggesting slightly later, syn-D<sub>2</sub> emplacement. Two coarse-grained, hornblende-rich diorite sills/dykes occur with only a very weak alignment of hornblende grains rendering the unit mostly massive. One thin, massive (i.e. non-foliated) microdiorite dyke may represent the last stage of diorite emplacement. A coarse-grained diorite dyke has been affected by D<sub>3</sub> folding, which indicates that some of the diorite dykes were emplaced between D<sub>2</sub> and D<sub>3</sub> events.

Across the Geita Hill gold deposit, numerous diorite sills and dykes occur that further constrain the relative time of emplacement. Figure 10 shows a thin (~1m wide) sill of hornblende diorite that is folded around D<sub>3</sub> folds along with the surrounding silicified sediments. Several other 10-15 m thick plagioclase-phyrlic diorite sheets also intruded parallel, or at low angles to bedding, and appear to be folded around the D<sub>3</sub> folds. However, these intrusions are discordant with layering near the fold hinges, and an apophysis of one of

the sills transects the antiformal hinge (Fig. 10). A second hornblende diorite dyke cuts both earlier diorite types and is dismembered by a later,  $D_6$  fault. This outcrop illustrates that emplacement of the diorite sills and dykes, continued during and post-dated  $D_3$  folding events.

Within the Nyankanga deposit to the SW of Geita Hill, the diorite sills and dykes merge into a large, massive diorite body, which contains rafts and xenoliths of multiply folded ironstone fragments (Sanislav et al. 2015). Viewed together, we interpret the diorite intrusive complex to be emplaced in a series of pulses, starting during the late stages of  $D_2$ , and extending until after  $D_3$  deformation was completed. It is not clear how  $D_4$  and  $D_5$  events affected the Nyankanga Intrusive Complex in the Nyankanga deposit, but these events appear to have folded the diorite sills in Geita Hill.  $D_6$  shear zones truncate and offset the various generations of diorite intrusions.

### 3.2.2 Lamprophyre dykes and deformation

Two generations of lamprophyre dykes have been recognised in the Geita Hill deposit: 1. rare, folded dykes (Fig. 9e) that are highly altered; and 2. dykes and sills that cut the folded sequence and are relatively fresh (Fig. 3; Borg 1994).

Figure 6 shows an example of an early lamprophyre sill emplaced along  $S_0/S_1$ , which was folded during  $D_3$  and contains a well developed  $S_3$  axial planar cleavage indicating a relative emplacement age event between  $D_2$  and  $D_3$ , concomitant with the early stages of diorite emplacement.

The second generation of lamprophyre dykes are less altered and contain medium-grained biotite booklets in a groundmass of fine-grained feldspar and amphibole/biotite. They trend mostly E-W (dipping steeply N;  $\sim 352/59^\circ$ , Fig. 9e) to NE-SW (dipping moderately NW;  $\sim 308/44^\circ$ ), and locally parallel the  $S_0/S_1$  compositional layering. Some of the

lamprophyre dykes, especially those that trend E-W, have been affected by D<sub>7</sub> dextral shear zones (Fig. 3), in which case they may be weakly altered (carbonate veining), foliated and boudinaged. Borg and Krogh (1999) dated a lamprophyre dyke, and interpreted as a second generation of lamprophyre dyke sampled from the underground workings at Geita Hill at 2644±3 Ma (single zircon U-Pb age)..

### **3.2.3 Porphyritic granodiorite dykes and deformation**

The sedimentary units and diorite sills in Geita Hill have been intruded by quartz-porphyry and quartz-feldspar porphyry dykes of granodioritic composition (Fig. 4e). Figure 7 shows two 5-15 m thick, feldspar porphyry sills that occur 100 m south of the deposit. They are massive to weakly foliated (containing S<sub>2</sub>), with one sill affected by D<sub>3</sub> folding. Within the Geita Hill deposit, dykes are rare and cut diorite sills and D<sub>2</sub>-D<sub>3</sub> folds. In the nearby Nyankanga deposit (Sanislav et al. 2015) quartz and quartz-feldspar porphyry dykes intrude the main diorite body. Here, some quartz-feldspar porphyries have been cut by N-dipping D<sub>6</sub> thrusts, whereas other quartz and quartz-feldspar porphyries truncate D<sub>6</sub> thrusts, and are cut by D<sub>7</sub> and D<sub>8</sub> faults.

Thus, field relationships suggest that the quartz-feldspar porphyry dykes were mostly emplaced at a similar time (and as part of) intrusion of the Nyankanga Intrusive Complex, i.e. between the waning stages of D<sub>2</sub> (developing a weak foliation) and before D<sub>6</sub>. A second generation of felsic dykes (most prominently exposed in the Nyankanga deposit) intruded between D<sub>6</sub> and D<sub>7</sub> (Sanislav et al., 2015).

## 4. Mineralization in relation to structure and intrusions

Mineralization in Geita Hill occurs near a network of fractures with complex, multi-stage, D<sub>6</sub>-D<sub>8</sub> histories (Fig. 10). In this section we will summarize some of the pertinent observations made from both underground workings and the open pit, and make use of ore body models to define the complex relationship between mineralization and the structural-intrusive scheme presented above (Table 1).

### 4.1 Distribution of mineralization

When viewing the overall distribution of mineralization of the Geita Hill gold deposit, a low grade (0.5 g/t) mineralization envelope can be defined along the length of the Geita Hill pit, which trends NE-SW, dips moderately NW and cuts across bedding and the diorite layers. Towards the SW end of the pit where the GHSZ terminates into a splay of minor fractures the ore envelope thins and terminates. The envelope appears to be largely confined to the short limb of a major D<sub>3</sub> fold pair mapped in the pit (Figs. 3 and 12). In places discrete shear zones can be found within the ore envelope, whereas elsewhere, no major shear occurs within the ore envelope. High-grade (>5 g/t) ore lenses generally plunge ~40-45° from W to NNE (Fig. 13a). They cluster around a common linear direction (~345/45; Fig. 13a) that approximately parallels the orientation of F<sub>3</sub> and F<sub>4</sub> fold hinges. In the NE part of the deposit, the plunge of the high grade lenses is consistently NW (Fig. 13b), whereas in the SW part of the deposit ore lenses show a larger range of orientations with plunge direction varying between W to NE (Fig. 13c).



## 4.2 Timing relationships for mineralization and alteration textures

In terms of alteration assemblages, gold is associated with pyrite-biotite-actinolite-carbonate-chlorite, and extensive quartz-carbonate veining within complexly fractured rocks (cf. Borg, 1994). Two main phases of pyrite textures have been described; an early, fine-grained anhedral to subhedral pyritic phase with abundant magnetite inclusions that occurs along broad alteration fronts replacing magnetite within the ironstone units, followed by a medium- to coarse-grained, euhedral, inclusion-free pyrite phase (Borg, 1994; Borg and Rittenauer, 2000), which represents a late tectonic overgrowth. According to Borg (1994), gold is predominantly contained as inclusions within the late euhedral pyrite grains and the gold mineralization postdates the emplacement of the lamprophyre dykes. The second generation lamprophyre dykes is overprinted by the D<sub>7</sub> deformation (Section 3.2.2) and the late pyrite overgrows all structural fabrics including the shears along the margins of late lamprophyre dykes (Borg, 1994), suggesting that most gold mineralisation post-dates D<sub>7</sub>. These observations are corroborated by structural overprinting relationships. D<sub>7</sub> structures displace the D<sub>6</sub> GHSZ (Figs. 3 and 6), but the 0.5 g/t ore envelope (Fig. 3) and the reef and stope patterns (Fig. 6) are undisturbed. These relationships suggest that the pre-existing D<sub>6</sub> shear zones provided ideal trapping structures, thus, controlling the localisation of gold mineralization along the D<sub>6</sub> GHSZ, but the time at which most mineralising fluids entered the shear zone may have occurred after D<sub>7</sub> (see also Sanislav et al., 2015)

Veins associated with the mineralized fracture zones are mm- to cm-thick features composed of quartz, quartz-sulfide and quartz-chlorite-sulfide-carbonate. Shearing has locally led to attenuation and brecciation of veins. Tension gashes are uncommon, but may occur within and adjacent to shear zones. Intense silicification and brecciation commonly coincides with high-grade mineralization. Hydrothermal brecciation (in situ fragmentation without rotation of the fragments) is locally important, and spatially restricted to zones of

intense alteration in both sedimentary rocks and diorite. Brecciation probably occurred late in the evolution of the deposit and was associated with intense silicic alteration, as indicated by the intense alteration of clasts. All clasts are silicified and no crosscutting, late quartz or carbonate veins were observed.

### **4.3 Mineralization and rock types**

All sedimentary and intrusive rock types described above host mineralization. However, some rock types are much more pervasively mineralized than others, reflecting a lithological control on mineralization. The bulk of the mineralization is contained within chert-magnetite-rich sedimentary rocks and within equigranular diorite, with the highest grades by far, concentrated along the contact between diorite and chert-magnetite-rich metasedimentary rocks. No discernible difference in gold grade distributions was observed within the several diorite types, and both types of lamprophyre dykes are mineralized. The felsic porphyry dykes are generally barren, although locally some of the porphyry dykes do contain gold.

### **4.4 Mineralization and structure**

Mineralization is spatially related to the Geita Hill Shear Zone, which consists of fault segments that terminate in splays of minor faults and fractures. The complex nature of the mineralized structures is illustrated in Figures 6, 10 and 11. In general it can be inferred that high-grade ore shoots also occur parallel to D<sub>3</sub> fold hinges (Fig. 10), and some early workers (e.g. Horne, 1957) interpreted the fracturing to be related to high strain intensities in the fold hinge zone. However, as shown in this paper, the fracture zones that occur along the D<sub>3</sub> fold hinges formed later and are not part of the folding events.

Figure 6 illustrates the link between mineralization and the complex pattern of fractures overprinting a D<sub>3</sub>, antiformal fold nose which plunges 335/44. The principal fracture, the D<sub>6</sub> GHSZ (~310/55) is mineralized along its length, with high grades (>5.0 g/t) occurring in discrete lenses. The largest lens of high-grade mineralization occurred where the shear zone changes orientation from a SW to a SSW strike (~200°), and a network of sub-parallel mineralized fractures converge with the shear trend (Fig. 6). The high-grade lens consists of a hydrothermal breccia with angular, variably altered metasediment fragments set in a quartz-carbonate-pyrite vein network, and plunges 353/43 (Carter 1959).

Further to the SW, mineralization is associated with gentle S-shaped, SW- to SSW-trending quartz veins (e.g. Carter, 1959; old mine plans). High-grade mineralized zones within workings are associated with a number of minor fractures, orientated 355/70, 322/70 (sinistral-reverse), and 045/59 (dextral-reverse), highlighted by the pattern of stopes (Fig. 6). Together these fractures form a broad zone of fracturing consistent with a sinistral-reverse Riedel, P-shear, anti-Riedel patterns. This fracture zone, which is of D<sub>6</sub> origin can be traced along the Geita Hill deposit with the late lamprophyre dykes cutting through these fractures.

When gold grades (>0.5 g/t and >5.0 g/t Au) are superimposed on geology within the deposit, the relationship between mineralization and structures can be further illustrated (Fig. 10). Three groups of faults are associated with mineralization and intense sulfidization, veining and alteration: 1. steeply NW to NNW dipping faults (~330/65); 2. moderately NW-dipping (~310/43) faults; and 3. steeply N-dipping faults (350/78), all recording a sinistral reverse movement of D<sub>6</sub> origin (Fig. 11e), and all affected by later reactivation. These orientations are identical to the orientation of on-reef stopes underground (Fig. 6). The faults commonly bound zones of high sulfidization and silica alteration. The bulk of the mineralization tends to lie between the faults in shallow dipping sigmoidal lenses, which cross-cut bedding, and which occur close to or along the lithological contact between

sedimentary rocks and intrusive diorite sills (Fig. 10). Some high-grade mineralization occurs within the faults and has a steeper dip. In these outcrops sampling shows that there is no clear link between the mineralized lenses and the D<sub>3</sub> fold nose.

## **5. Discussion**

### **5.1 The tectonic history of the greenstone belt**

A summary of the deformation and intrusive events encountered in the Geita Hill deposit and the surrounding rocks is presented in Table 1. Based on available age constraints, geological events following deposition of the sedimentary sequence can be subdivided into two groups, or tectonic episodes: 1. an early (2700-2680 Ma) episode of deformation involving D<sub>1</sub>-D<sub>6</sub> events broadly coeval with the emplacement of lamprophyre, diorite and porphyritic granodiorite dykes and sills; and 2. a late episode (<2645 Ma) of lamprophyre dyke emplacements followed by D<sub>7</sub>-D<sub>8</sub> brittle-ductile shearing events and mineralization. This latter group of events coincides with the emplacement of 2620-2660 Ma granitoids to the east, north and west of the GGB (Sanislav et al. 2014), and marks the final stages of deformation and igneous activity (Sanislav et al., 2015).

The early D<sub>1</sub>-D<sub>2</sub> events in the Geita area may have started during deposition of the sedimentary sequence. The presence of secondary magnetite (and pyrite) banding and silicification resulting in chert layers, overprinting precursor sedimentary rocks is generally interpreted to result from early diagenetic and volcanic alteration processes, partly during periods of non-deposition of turbidite (Borg and Rittenauer 2000; Krapez et al. 2003). However, it is possible that these early alteration features may have been wholly, or partly, imparted by tectonic processes with fluids channelled along layer-parallel structures during

early stages of burial in which some of the chert horizons may have originated as layer-parallel quartz veins (e.g. Hofmann et al. 2001, 2003). The mylonitic, D<sub>1</sub> chert horizons with internal disharmonic folds observed in and around the Geita Hill deposit (Fig. 7) may represent such early D<sub>1</sub> shears, similar to early shears described in other greenstone belts around the world (e.g. Weinberg and van der Borgh 2008; Dirks et al. 2009), where they are commonly interpreted as early thrusts, duplicating stratigraphy (Hofmann et al. 2001; 2003; Weinberg and van der Borgh 2008).

It is likely that D<sub>1</sub> and D<sub>2</sub> events were progressive in nature. The initial D<sub>1</sub>, layer-parallel non-coaxial deformation, resulted in boudinaging of chert horizons in fine-grained magnetite-rich shales, with deformation progressively becoming coaxial during D<sub>2</sub> with boudin-trains being folded around non-cylindrical D<sub>2</sub> folds (Fig. 7). If combined with the observation that most F<sub>2</sub> folds have a Z-vergence within plan view, this would suggest that D<sub>1</sub>-D<sub>2</sub> events could have resulted from transpressional deformation, with a significant non-coaxial, sinistral component.

Borg et al. (1990) proposed that the Sukumaland Greenstone Belt experienced an early (D<sub>1borg</sub>) deformation that produced open, tight and locally isoclinal folds with sub-horizontal axes, overprinted by a second period of folding (D<sub>2borg</sub>) that produced open and concentric folds with sub-vertical axes. We could not directly identify the early sub-horizontal folds proposed by Borg et al. (1990) in the Geita Hill region, but it is likely that they represent the D<sub>2</sub> folds described here. The D<sub>2borg</sub> folds described by Borg et al. (1990) were identified as the main folding structures at Geita Hill deposit by Borg (1994) and represent our D<sub>3</sub> folds. We could not identify the later E-W folding overprint seen by Borg (1994) at Geita Hill, but based on its description this folding event corresponds most probably to what we describe as D<sub>4</sub> folds, which locally trend E-W in other parts of the GGB (e.g. Kukuluma area).

D<sub>3</sub>-D<sub>4</sub> events affected D<sub>1</sub> and D<sub>2</sub> structures and refolded them around a generally NW-plunging axis. It is common in many greenstone terrains that early, layer-parallel shear zones are overprinted by later, more upright folding events that resulted in large-scale synformal geometries that characterise the architecture of many greenstone belts (e.g. Peterson and Zaleski 1999; Hofmann et al. 2003; de Witt et al. 2011; Bedard et al. 2013; Lin and Beakhouse 2013), and D<sub>3</sub> and D<sub>4</sub> events may represent these structures. D<sub>5</sub> recumbent folds and associated horizontal fracturing also represent a group of structures common in many greenstone belts, and have been linked to diapiric doming, and cascade folding (e.g. Jelsma et al. 1996; Lin and Beakhouse 2013) as diapirs intruded along the margins of greenstone belts.

The network of D<sub>6</sub> reverse-sinistral shear zones share common features with earlier ductile structures, suggesting that the D<sub>6</sub> shears represent the retrograde, waning stages of the first deformation episode. Intersection lineations between different sets of D<sub>6</sub> shear zones are (sub-)parallel to D<sub>3</sub> and D<sub>4</sub> fold axes, and the dominant D<sub>6</sub> fracture trend generally parallels S<sub>0</sub>/S<sub>1</sub>, and appears to concentrate along D<sub>3</sub> fold axial planes (Fig. 9c). D<sub>6</sub> shear zones commonly have a sinistral displacement component consistent with the prevalence of S-folds of D<sub>1</sub>-D<sub>2</sub> and even D<sub>3</sub> origin. The fact that in the nearby Nyankanga deposit, quartz porphyry dykes dated at  $2689 \pm 11$  Ma (Chamberlain and Tosdal 2007; Sanislav et al., 2015) truncate D<sub>6</sub> shear zones further strengthens the close timing relationship between the formation of the D<sub>6</sub>, reverse sinistral shear zones and earlier (D<sub>2-5</sub>), ductile deformation events, and constrains the overall timing of this deformation episode to the 2700-2680 Ma age bracket.

## 5.2 Timing of gold mineralization at Geita Hill

Because of the complexity of the structural-intrusive history, reports on the relationship between mineralization, structure and intrusions can be contradictory depending on where observations are made. In general Geita Hill is classified as an Archean, BIF-hosted, orogenic gold deposit linked to secondary structures related to major thrusts, with mineralization being younger than 2644 Ma (Borg and Krogh 1999), but this interpretation is based on limited published structural work.

Mineralization at Geita Hill is spatially linked to the Geita Hill Shear Zone, which is a sinistral reverse shear zone with an anastomosing nature composed of a set of complex and narrow (<10 cm), D<sub>6</sub>, structures with no significant (i.e. <10m) displacements. Earlier work by Borg (1994) mentioned the lack of lateral displacement associated with this shear zone and the spatial correlation between the gold mineralization and the trace of the shear zone. Because mineralization is spatially associated with this network of sinistral reverse shear zones, it is commonly assumed that thrust-stacking (Painter, 2004) controlled mineralization, and that the Geita Hill deposits are shear zone controlled orogenic gold deposits. As our observations have demonstrated, the relationship between the reverse faults and mineralization is more complex, D<sub>6</sub> sinistral reverse shear zones only accommodated modest displacements (< 5m), and were not responsible for the formation of thrust stacks or duplex structures, and the main phase of mineralisation post-dated the D<sub>6</sub> shearing event, in which D<sub>6</sub> shears provide suitable trapping structures, but do not control the timing of events.

In general, mineralization at Geita Hill can be linked to a NE-trending network of deformation zones, which include prominent, layer-parallel, moderately NW-dipping brittle-ductile shear zones that are discontinuous along strike and locally mineralized. The shear zones are characterised by a multi-staged deformation history with only minor displacements involving early sinistral reverse movement (D<sub>6</sub>), and later dextral or sinistral (D<sub>7</sub>) and normal

movements ( $D_8$ ), with  $D_6$  (~2690 Ma) and  $D_{7-8}$  (<2645 Ma) occurring at different times (Table 1). The shear zones originated during  $D_6$  as sinistral reverse faults, and only some of the  $D_6$  shear zones in the pit are mineralized.

The main phase of mineralization at Geita Hill appears to be younger, because late-tectonic (2644 Ma) lamprophyre dykes have been sheared, are overprinted by the second phase of euhedral, gold-bearing pyrite, and are mineralized (Borg, 1994). Therefore, although the  $D_6$  sinistral reverse shear zones are preferentially mineralized, the main phase at which mineralizing fluids entered these shear zones occurred long after their formation, presumably because they presented suitable fluid conduit and trapping structures within the prevailing stress field at the time mineralizing fluids entered the greenstone pile. This appears to have happened after  $D_6$  shearing, at a time the greenstone belt experienced extensive igneous activity along its margins (Sanislav et al. 2014). Based on the observations that mineralization is texturally late (Borg, 1994), and that the last stage of deformation is  $D_8$  normal faulting, which has reactivated at least some of the sinistral reverse shear zones, gold deposition could have been coeval with  $D_8$  normal faulting events, i.e. at a stage the greenstone belt experienced regional extension due to events unrelated to the accretionary history of the belt (cf. Dirks et al. 2013). This is consistent with the nearby Nyankanga deposit, which also displays ore zone geometries consistent with normal movement as reactivation on earlier  $D_6$  thrusts (Sanislav et al. 2015).

If gold-bearing fluids were late-tectonic in origin, why were only certain  $D_6$  shear zones mineralized and others not? The same situation appears to arise in the nearby Nyankanga deposit, where ironstone intruded by extensive diorite is transected by a network of N- to NW-dipping sinistral thrusts of which only a few are spatially associated with mineralization (Sanislav et al. 2015). This preferential mineralization of certain  $D_6$  shear zones suggests the presence of additional controls, such as overprinting structures of  $D_7$  or  $D_8$



origin that reactivated or cross-cut D<sub>6</sub> thrusts and interacted with them in particular areas. Thus, only certain parts of D<sub>6</sub> structures, where affected by reactivations during D<sub>7</sub> or D<sub>8</sub>, would have provided the right heterogeneity to create suitable mineralization traps (Sanislav et al., 2015) during the influx of mineralising fluids. It is noted that D<sub>8</sub> fractures are generally minor and associated with few deformation features other than narrow shear joints. The nature of any larger scale D<sub>8</sub> structure potentially associated with mineralization has not been clearly defined within the deposits.

### **5.3 The role of iron-rich rocks (ironstones and diorite) in precipitating gold**

Gold mineralization in the Geita Hill deposit can be found in all rock types; however, ironstone is the main host rock type to mineralization with diorite intrusions second to ironstone. This close relationship between gold mineralization and iron-rich host rocks suggests that the host rock composition played an important role in the gold precipitation process. Gold mineralization is genetically related to the sulfide alteration (e.g. Borg, 1994) and is restricted to the damage zone associated with the Geita Hill Shear Zone. Gold values and associated sulfide alteration transition from high gold values and intense sulphide alteration to barren, unaltered ironstone over a few meters (Borg and Rittenauer, 2000). This suggests that gold deposition was triggered by sulfidation reactions in chemically reactive, iron-rich host rocks (ironstone and diorite). Borg and Rittenauer (2000) proposed that the sulfidation of magnetite resulted in the oxidation of the sulfur-rich, auriferous fluid and caused the precipitation of gold. High sulfur activity of the mineralizing fluid fixed the auriferous pyrite (Borg, 1994) in the ironstone by consuming Fe<sup>2+</sup> (Adomako-Ansah et al., 2013). The reducing ore fluid was between 350-400°C (Borg, 1994) and reacted with the Fe from the wall rock to form pyrite and release oxygen, which in turn made the fluid precipitate the gold from solution. However, the whole rock reaction of the mineralizing fluid with

chemically reactive ironstone cannot solely account for all the precipitated gold and sulfide. Besides the gold-bearing replacement textures seen in the ironstone, gold mineralization is also common in hydrothermal breccia zones where phase separation during fault movement can be inferred as the main precipitation mechanism (e.g. Weatherley and Henley, 2013). Note that prior to 2002 when the open pit mining commenced, Geita Hill deposit was mined underground with mining being focused on the high grade hydrothermal breccia and veins. Based on the descriptions found in the mine records (e.g. Carter 1959) these are hydraulic breccias. This suggests that the processes responsible for the formation of these hydrothermal breccia and veins contributed to gold deposition from the mineralized fluid. The replacement of iron-rich silicate minerals in diorite by auriferous pyrite and the subsequent silica release can account for some of the silicification associated with the mineralization (Gregor Borg – personal communication).

#### **5.4 Controls on gold mineralization**

Based on the observations made in this paper, the following geological factors control the distribution and grade of mineralization that must be considered in any genetic model for the deposit:

1. Mineralization has been shown to parallel shear zones that first formed during D<sub>6</sub>, with the GHSZ being the most prominent, i.e. D<sub>6</sub> shear zones control the localisation of mineralization;

2. In detail, most mineralization does not actually occur within the shear zones, but it rather occurs in fine fractures within a damage zone that envelops the shear zones and controls zones of alteration and mineralization within the wall rocks (Fig. 10), i.e. shear zones are fluid conduits rather than trapping structures.

3. The age of some, if not all, mineralization is potentially younger than the ductile shear system that facilitated the mineralization, and gold-bearing fluids may have been

introduced during a late tectonic episode possibly coincident with normal, brittle faulting and extension of the greenstone belt.

4. The generally NW-plunging, high-grade ore shoots (Fig. 13a, b and c) parallel  $D_3$  and  $D_4$  fold axes, and  $D_3$  fold axial planes (Fig. 13d), intersection lineations between  $D_6$  shear segments (Fig. 13 d to h) and  $S_0/S_1$  orientations, i.e. mineralization trends are controlled by underlying intersections of  $D_1$ - $D_6$  structures, which create a permeable architecture in the rock mass guiding fluid flow, or put differently, pre-existing structures played an important role in the localization of the Geita Hill Shear Zone and high grade ore shoots, and controlling their ore body geometry;

5. The highest gold grades are associated with the sulfidation reactions along diorite-ironstone contacts and locally developed pyritic hydrothermal breccia zones, and quartz-carbonate veining, as well as a wide alteration zone, i.e. mineralization is linked to an episode of major fluid ingress possibly related to intrusive activity at depth;

6. Mineralization is best developed in iron rich units with extensive pyrite alteration of the magnetite in ironstones and the amphiboles in diorite, i.e. mineralization is host-rock controlled (cf. Borg and Rittenauer, 2000).

7. In detail (Fig. 10) many ore lenses occur along the contacts between ironstone and diorite bodies, i.e. mineralization appears preferentially near the lithological boundary between diorite and ironstone, which constitutes a compositional difference.

8. Mineralization may be associated with later-stage reactivation of certain  $D_6$  shear zones during  $D_8$  extension, although there is limited evidence for the presence of large-scale  $D_8$  structures.

## 5.5 A model for gold mineralization and conclusions

The Geita Hill gold deposit shares many characteristics with typical orogenic gold deposits, e.g. its association with quartz-veins (although of limited extent and missing in many levels), complexly deformed ironstone near shear zones, the absence of an obvious igneous genetic relationship to intrusions (despite the presence of abundant diorite) and greenschist facies alteration patterns. However, as discussed, the timing of the principle phase of mineralization post-dates the ductile deformation events in the GGB, interpreted as accretionary (e.g. Kabete et al. 2012), by tens of millions of years, and therefore, mineralization appears to be post-orogenic, and the link to orogenic processes (i.e. subduction-accretion) is tenuous at best. Instead it is proposed that mineralization was introduced during an extensional phase of deformation that broadly coincided with the final igneous events to affect this part of the Tanzania Craton, before the craton stabilised (e.g. Sanislav et al., 2015; Dirks et al. 2013).

In summary, our current understanding of Geita Hill gold deposit suggests that the deposit is hosted by deformed supracrustal rocks that occur above a large diorite intrusion (Fig. 5) that is part of the Nyankanga Intrusive Complex. The supracrustal package is dominated by folded banded ironstone and turbiditic sediments intruded at various times during the tectonic history by diorite dykes and sills originating from the large diorite body (Nyankanga Intrusive Complex) at depth. The mineralization envelope is spatially associated with the D<sub>6</sub> Geita Hill Shear Zone, which is at Geita Hill occurs in close spatial association with D<sub>3</sub> folds axial planes (Fig. 12). The intersection of the Geita Hill Shear Zone with different structural elements provided ideal mineralization conduits with diorite-ironstone contacts providing the best depositional sites for gold.

## Acknowledgements

The authors would like to acknowledge Geita Gold Mine and AngloGold Ashanti for financial support and for allowing publication of this work. In depth reviews by Gregor Borg, David Lentz and an anonymous reviewer are greatly acknowledged.

## Bibliography

- Adomako-Ansah K, Mizuta T, Hammond NQ, Ishiyama D, Ogata T, Chiba H (2013) Gold Mineralization in Banded Iron Formation in the Amalia Greenstone Belt, South Africa: A Mineralogical and Sulfur Isotope Study. *Resource Geology* 63: 119-140.
- Bierlein FP, Groves DI, Cawood PA (2009) Metallogeny of accretionary orogens - The connection between lithospheric processes and metal endowment. *Ore Geology Reviews* 36: 282-292.
- Blenkinsop TG (2004) Orebody geometry in lode gold deposits from Zimbabwe: implications for fluid flow, deformation and mineralization. *Journal of Structural Geology* 26: 1293–1301.
- Blenkinsop TG, Oberthür T, Mapeto O (2000) Gold mineralization in the Mazowe area, Harare-Bindura-Shamva greenstone belt, Zimbabwe: I. Tectonic controls on mineralization. *Mineralium Deposita* 35: 126–137.
- Blewett RS, Czarnota K, Henson PA, Champion DC (2010) Structural-event framework for the eastern Yilgarn Craton, Western Australia, and its implications for orogenic gold: *Precambrian Research* 183: 203–229
- Borg G (1992) New aspects on the lithostratigraphy and evolution of the Siga Hills, an Archaean granite-greenstone terrain in NW-Tanzania. *Zeitschrift für Angewandte Geologie* 38: 89-93.

851 Borg G (1994) The Geita gold deposits, NW-Tanzania. *Geology, ore petrology, geochemistry*  
852 and timing of events. *Geologisches Jahrbuch* 100: 545–595.

853 Borg G, Lyatuu DR, Rammlmair D (1990) Genetic aspects of the Geita and Jubilee reef,  
854 Archean BIF-hosted gold deposits, Tanzania. *Geologische Rundschau* 79: 355–371.

855 Borg G, Shackleton RM (1997) The Tanzania and NE Zaire Cratons. In: de Wit, M.J., Ashwal,  
856 L.D. (Eds.) *Greenstone Belts*. Clarendon Press, Oxford, pp. 608-619.

857 Borg G, Krogh T (1999) Isotopic age data of single zircons from the Archaean Sukumaland  
858 Greenstone Belt, Tanzania. *Journal of African Earth Sciences* 29: 301-312

859 Borg G, Rittenauer A (2000) Syn - and epigenetic sulphides in Archean BIFs of NW -  
860 Tanzania and their significance to gold mineralization. . In: Rammlmair et al. (eds)  
861 *Applied Mineralogy*, Balkema, Rotterdam, 263 - 266.

862 Carter GS (1959) Exploration at Geita and NE extension mines. Geological Survey of  
863 Tanganyika. Report No. GSC/7.

864 Cassidy KF, Groves DI, McNaughton N,J (1998) Late Archean granitoid-hosted lode-gold  
865 deposits, Yilgarn Craton, Western Australia: Deposits characteristics, crustal architecture  
866 and implications for ore genesis. *Ore Geology Reviews* 13: 65-102.

867 Chamberlain CM, Tosdal RM (2007) U–Pb geochronology of the Lake Victoria Greenstone  
868 Terrane, Tanzania. Mineral Deposit Research Unit The University of British Columbia  
869 (Research Program on World-class Gold Deposits and Advanced Exploration Projects  
870 Owned and/or Joint Ventured to Barick Gold, Placer Dome, Anglo-Gold Ashanti,  
871 Resolute Mining NL as Main Sponsors.

872 Cloutier J, Stevenson RK, Bardoux M (2005) Nd isotopic, petrologic and geochemical  
873 investigation of the Tulawaka East gold deposit, Tanzania Craton. *Precambrian Research*  
874 139: 147-163.

875 Colvine AC, Fyon JA, Heather KB, Marmont S, Smith PM, Troop DG (1988) Archaean lode  
876 gold deposits in Ontario. Ontario Geological Survey, Ontario, Canada. Miscellaneous  
877 Paper 139, pp. 136.

878 Cowley PN 2001. The discovery and development of the Geita gold deposits, Northern  
879 Tanzania. in Yates K (Ed.). NewGenGold 2001. Conference Proceedings AMF, Adelaide.  
880 123-135.

881 de Wit MJ, Furnes H, Robins B (2011) Geology and tectonostratigraphy of the Onverwacht  
882 Suite, Barberton Greenstone Belt, South Africa. Precambrian Research 186: 1–27.

883 Dirks PHGM, Charlesworth EG, Munyai MR (2009) Cratonic extension and Archaean gold  
884 mineralization in the Sheba-Fairview mine, Barberton Greenstone Belt, South Africa.  
885 South African Journal of Geology 112: 291–316.

886 Dirks PHGM, Charlesworth EG, Munyai MR, Wormald RJ (2013) Stress analyses, post-  
887 orogenic extension and 3.01 Ga gold mineralization in the Barberton Greenstone Belt,  
888 South Africa. Precambrian Research 226: 157-184.

889 Forbes CJ, Betts PG, Lister GS, (2004) Synchronous development of Type 2 and Type 3 fold  
890 interference patterns: evidence for recumbent sheath folds in the Allendale Area, Broken  
891 Hill, NSW, Australia. Journal of Structural Geology 26: 113–126

892 Gabert G (1990) Lithostratigraphic and Tectonic Setting of Gold Mineralization in the Archean  
893 Cratons of Tanzania and Uganda, East Africa. Precambrian Research 46: 59-69.

894 Goldfarb RJ, Groves DI, Gardoll S (2001) Orogenic gold and geologic time: a global synthesis.  
895 Ore Geology Reviews 18: 1–75.

896 Goldfarb RJ, Groves DI, Taylor RD, Deb M (2010) Controls on the global distribution of  
897 orogenic gold and their significance relative to India, *in* Deb, M. and Goldfarb, R.J.,  
898 editors, Gold Metallogeny: India and Beyond, Alpha Science International, Oxford, UK,  
899 p. 48-57.

900 Graseman B, Wiesmayr G, Draganits E, Füsseis F (2004) Classification of refold structures.  
 901 Journal of Geology 112: 119-125.

902 Groves DI, Goldfarb RJ, Gebre-Mariam M, Hagemann SG, Robert F (1998) Orogenic gold  
 903 deposits: a proposed classification in the context of their crustal distribution and  
 904 relationship to other gold deposit types. Ore Geology Reviews 13: 7–27.

905 Groves DI, Goldfarb RJ, Robert F, Hart C (2003) Gold deposits in metamorphic belts: Current  
 906 understanding, outstanding problems, future research and exploration significance.  
 907 Economic Geology 98: 1-30.

908 Hagemann SG, Groves DI, Ridley JR, Verncombe JR (1992) The Archean lode-gold deposits  
 909 at Wiluna, Western Australia: high level brittle-style mineralization in a strike-slip  
 910 regime. Economic Geology 87: 1022–1053.

911 Hofmann A, Dirks PHGM, Jelsma HA (2001) Horizontal tectonic deformation geometries in a  
 912 late Archaean sedimentary sequence, Belingwe greenstone belt, Zimbabwe. Tectonics  
 913 20: 909-932.

914 Hofmann A, Dirks PHGM, Jelsma HA, Matura N (2003) A tectonic origin for ironstone  
 915 horizons in the Zimbabwe Craton and their significance for greenstone belt geology.  
 916 Journal Geological Society of London 160: 83-97.

917 Horne RG (1959) Notes on the structure at Geita mine. Geological Survey of Tanganyika.  
 918 Report No. RGH/1.

919 Hronsky JMA, Groves DI, Loucks RR, Begg GC (2012) A unified model for gold  
 920 mineralization in accretionary orogens and implications for regional-scale exploration  
 921 targeting. Mineralium Deposita 47: 339-358.

922 Jelsma HA, Vinyu ML, Valbracht PJ, Davies GR, Wijbrans JR, Verdurmen EAT (1996)  
 923 Constraints on Archaean crustal evolution of the Zimbabwe Craton: a U-Pb zircon, Sm-



924 Nd and Pb-Pb whole-rock isotope study. *Contributions to Mineralogy and Petrology* 124:  
 925 55–70.

926 Junqueira PA, Lobato LM, Ladeira EA, Simoes EJM (2007) Structural controls and  
 927 hydrothermal alteration at the BIF-hosted Raposos lode-gold deposit, Quadrilatero  
 928 Ferrifero, Brazil. *Ore Geology Reviews* 32: 629-650.

929 Juul-Pedersen A, Frei R, Appel PWU, Persson MF, Konnerup-Madsen J (2007) A shear zone  
 930 related greenstone belt hosted gold mineralization in the Archean of West Greenland. A  
 931 petrographic and combined Pb–Pb and Rb–Sr geochronological study. *Ore Geology*  
 932 *Reviews* 32: 20–36.

933 Kabete JM, Groves DI, McNaughton NJ, Mruma AH (2012) A new tectonic and temporal  
 934 framework for the Tanzanian Shield: implications for gold metallogeny and  
 935 undiscovered endowment. *Ore Geology Reviews* 48: 88-124.

936 Krapež B, Barley ME, Pickard AL (2003) Hydrothermal and resedimented origins of the  
 937 precursor sediments to banded iron formations: sedimentological evidence from the early  
 938 Palaeoproterozoic Brockman Supersequence of Western Australia. *Sedimentology* 50:  
 939 979-1011.

940 Kuehn S, Ogola J, Sango P (1990) Regional setting and nature of gold mineralization in  
 941 Tanzania and southwest Kenya. *Precambrian Research* 46: 71-82.

942 Kwelwa S, Many S, Vos INA (2013) Geochemistry and petrogenesis of intrusions at the  
 943 Golden pride gold deposit in the Nzega greenstone belt, Tanzania. *Journal of African*  
 944 *Earth Sciences* 86: 53-64.

945 Leclair AD, Ernst RE, Hattori H (1993) Crustal-scale auriferous shear zones in the central  
 946 Superior province, Canada. *Geology* 21: 399-402.

947 Lin S, Beakhouse GP (2013) Synchronous vertical and horizontal tectonism at late stages of  
 948 Archean cratonization and genesis of Hemlo gold deposit, Superior craton, Ontario,  
 949 Canada. *Geology* 41: 359 – 362.

950 Maboko MAH, Pedersen RB, Manya S, Torssander P, Mwache M (2006) The origin of late  
 951 Archaean granitoids in the Sukumaland greenstone belt of northern Tanzania:  
 952 geochemical and isotopic constraints. *Tanzania Journal of Science* 32: 75–86.

953 Manya S (2004) Geochemistry and petrogenesis of volcanic rocks of the Neoarchaean  
 954 Sukumaland greenstone belt, northwestern Tanzania. *Journal of African Earth Sciences*  
 955 40: 269–279.

956 Manya S, Maboko MAH (2003) Dating basaltic volcanism in the Neoarchaean Sukumaland  
 957 Greenstone Belt of the Tanzania Craton using the Sm–Nd method: implications for the  
 958 geological evolution of the Tanzania Craton. *Precambrian Research* 121: 35–45.

959 Manya S, Maboko MAH (2008) Geochemistry of the Neoarchaean mafic volcanic rocks of the  
 960 Geita area, NW Tanzania: implications for stratigraphical relationships in the  
 961 Sukumaland greenstone belt. *Journal of African Earth Sciences* 52: 152–160.

962 Miller J, Blewett R, Tunjic J, Connors K (2010) The role of early formed structures on the  
 963 development of the world class St Ives Goldfield, Yilgarn, WA. *Precambrian Research*  
 964 183: 292–315.

965 Painter M (2004) Mineralization and structural architecture of the Geita Hill Shear Zone.  
 966 Unpublished Geita Gold Mine internal report.

967 Peterson VL, Zaleski E (1999) Structural history of the Manitouwadge greenstone belt and its  
 968 volcanogenic Cu–Zn massive sulphide deposits, Wawa subprovince, south-central  
 969 Superior Province. *Canadian Journal of Earth Sciences* 36: 605–625

970 Quenell AM, McKinlay AC, Aitken WG (1956) Summary of the geology of Tanganyika, part  
 971 1. Geological Survey of Tanganyika Memoirs, 1–26.

972 Ribeiro-Rodrigues LC, De Oliveira CG, Friedrich G (2007) The Archean BIF-hosted Cuiaba  
 973 Gold deposit, Quadrilatero Ferifero, Minas Gerais, Brazil. *Ore Geology Reviews* 32:  
 974 543-570.

975 Robert F, Sheahan PA, Green SB (1991) *Greenstone Gold and Crustal Evolution*. Publication  
 976 of the Mineral Deposits Division, Geological Association of Canada, 252pp.

977 Sanislav IV, Wormald RJ, Dirks PHGM, Blenkinsop TG, Salamba L, Joseph D (2014) Zircon  
 978 U-Pb ages and Lu-Hf isotope systematics from late-tectonic granites, Geita greenstone  
 979 belt: implications for crustal growth of the Tanzania craton. *Precambrian research* 242:  
 980 187-204.

981 Sanislav IV, Kolling SL, Brayshaw M, Cook YA, Dirks PHGM, Blenkinsop TG, Mturi MI,  
 982 Ruhega R (2015). The geology of the giant Nyankanga gold deposit, Geita Greenstone  
 983 Belt, Tanzania. *Ore Geology Reviews* 69: 1-16.

984 Stokes TR, Zentilli M, Culshaw N (1990) Structural and lithological controls of gold bearing  
 985 quartz breccia zones in Archean metaturbidites, Gordon Lake, Northwest Territories,  
 986 Canada. *Canadian Journal of Earth Sciences* 27: 1577-1589.

987 Tripp GI, Vearncombe JR (2004) Fault/fracture density and mineralization: a contouring  
 988 method for targeting in gold exploration. *Journal of Structural Geology* 26: 1087–1108.

989 Vos IMA, Bierlein FP, Standing JG, Davidson GJ (2009) The geology and mineralization at  
 990 the Golden Pride gold deposit, Nzega greenstone belt, Tanzania. *Mineralium Deposita*  
 991 44: 751–764.

992 Walraven F, Pape J, Borg G (1994) Implications of Pb-isotopic compositions at the Geita gold  
 993 deposit, Sukumaland Greenstone Belt, Tanzania. *Journal of African Earth Sciences* 18:  
 994 111–121.

995 Weatherley DK and Henley RW (2013) Flash vaporization during earthquakes evidenced by  
 996 gold deposits: *Nature Geoscience* 6: 294-29.

997 Weinberg RF, van der Borgh P (2008) Extension and gold mineralization in the Archaean  
998 Kalgoorlie Terrane, Yilgarn Craton. *Precambrian Research* 161: 77–88.

999 Witt WK, Vanderhor F (1998) Diversity within a unified model for Archaean gold  
1000 mineralization in the Yilgarn Craton of Western Australia: an overview of the late-  
1001 orogenic, structurally-controlled gold deposits. *Ore Geology Reviews*: 29–64.

1002

## **Figure captions**

### **Figure 1**

Simplified geological map of the Lake Victoria region showing the main geological units (modified from Sanislav et al. 2015). SU – Sukumalanad Greenstone Belt; NZ – Nzega Greenstone Belt; SM – Shynianga-Malita Greenstone Belt; IS – Iramba-Sekenke Greenstone Belt; KF – Kilimafedha Greenstone Belt; MM – Musoma-Mara Greenstone Belt. Super-terrane boundaries are as proposed by Kabete et al. 2012a: ELVST – East Lake Victoria, MLEST- Mwanza Lake Eyasi, LNST- Lake Nyanza, MMST – Moyowosi-Manyoni, DBST – Dodoma Basement, MAST – Mbulu-Masai, NBT – Nyakahura-Burigi. Inset map of Africa showing the location of Archean blocks.

### **Figure 2**

Geological map of the Geita Greenstone Belt showing the main geological units (modified after Sanislav et al. 2015).

### **Figure 3**

Geological map (a) of the Geita Hill gold deposit (in the map background represented with thin lines is the pit wireframe; closed space lines show steep wall faces while wider spaced lines show less steep wall faces and benches) and geological cross section (b) along line A-A'. The symbols in (a) and (b) are the same unless otherwise specified. The deposit geology is dominated by ironstones intruded at various times mainly by diorite sills and dykes and subordinate lamprophyres and minor quartz-porphyrries of granodioritic composition. For section B-B' see Figure 10 and for section C-C' see Figure 11a. The location of figures 6 and 7 relative to the Geita Hill deposit are shown. Note that the location of Figure 6 is approximate since the level shown in the figure is not yet exposed.

**Figure 4**

Photographs showing the main lithological units in the Geita Hill gold deposit. a) ironstone formed by intercalations of chert and magnetic shales; b) transition from ironstone to laminated sandstones; c) detail of a plagioclase-rich diorite dyke from the Geita Hill gold deposit; d) diorite sub-parallel to ironstone bedding on the eastern side of the Geita Hill gold deposit (bench height is 5 m); e) late quartz-porphyry (granodioritic) dyke crosscutting the ironstones; f) sheared lamprophyre sub-parallel to bedding in ironstones

**Figure 5**

Schematic cartoon illustrating the relationship between Nyankanga Intrusive Complex, Nyankanaga deposit and Geita Hill deposit.

**Figure 6**

Underground geological plan (level 1395 m above sea level; redrawn and reinterpreted from mine records based on recent drilling) at the Geita Hill gold deposit. We use the distribution of stopped areas as a proxy for the distribution of gold mineralization. The old underground mining took out a reef with a cut-off grade of 8 g/t. The workings are dominated by metasediments folded in a D<sub>3</sub> synform plunging 335/44 in the NE and 353/39 in the SW (the stereoplots show poles to bedding measurements from both limbs). A prominent D<sub>6</sub> shear (~310/55; GHSZ) located along the NW limb of the synform has a strike extent of ~180m. The shear truncates and offsets the D<sub>3</sub> fold axis. The inset at the top of the figure shows the theoretical orientation of a system of fractures/shears that can develop in a deformation zone during sinistral shearing: Y – fractures/shears parallel to the shear zone boundary; R – Riedel

shears; R' – anti-Riedel shears; P – P shears; T – tension gashes. See text for detailed discussion.

## **Figure 7**

Detailed mapping along a road cut just outside the Geita Hill gold deposit containing most of the structural observations made in the Geita Hill deposit. Road cut symbol shows inclined surfaces dipping towards the road. a) Stereoplot showing bedding measurements as great circles and poles to bedding planes (black circles). The red square represents the mean vector. b) Stereoplot of D<sub>2</sub> fold axes (black circles) and the best fit great circle. The red squares represent the location of the eigen values calculated with a Bingham distribution. c) Stereoplot of D<sub>1</sub> lineations (black circles). d) Stereoplot showing the orientation of bedding (in D<sub>4</sub> folds) as great circles and as poles to bedding planes (black circles) with the cylindrical best fit and the fracture cleavage to D<sub>4</sub> as dashed lines. The red squares represent the location of the eigen values calculated with a Bingham distribution; e) Stereoplot of dextral shear zones as great circles and of the lineations on the fault planes as black circles.

## **Figure 8**

Photographs showing examples of the main structural elements observed in and around the Geita Hill pit. a) strongly boudinaged chert bands aligned along S<sub>0</sub>/S<sub>1</sub> are folded in tight D<sub>2</sub> folds in bedded chert ironstone unit; b) Transposed, D<sub>1</sub>, intrafolial fold of boudinaged chert bands aligned along S<sub>0</sub>/S<sub>1</sub>, with a S-vergence; c) D<sub>2</sub> sheath fold; d) example of D<sub>2</sub> fold overprinted by D<sub>3</sub>. Inset shows the interpretation of the fold overprinting relationships; e) large gentle upright D<sub>4</sub> fold highlighted by bedding undulations along subvertical axial

planes, with NW plunging fold axis. Note cross-cutting, flat  $S_5$  fracture cleavage; f) open  $D_5$  folds highlighted by bedding undulations along subhorizontal axial surfaces. Note the flat  $S_5$  fracture cleavage; g) striations and steps on a  $D_6$  fault surface within the GHSZ showing sinistral reverse oblique movement; h) example of discrete,  $D_8$  fault showing normal movement (inset shows the interpretation of the shear sense). These fracture zones with normal movement affected and reactivated  $D_6$  shear zones.

#### **Figure 9**

Stereoplots of a) poles to bedding; b)  $D_2$  folds plunges (black dots plotting along a great circle similar in orientation to the axial plane of the  $D_3$  folds) and of  $D_3$  folds plunges (white filled circles; the shaded area shows the spread of  $D_3$  folds plunges which, consistently plunge NW); poles to diorite contacts; and c) of folds axial planes from Geita Hill deposit. Stereoplots of poles to the diorite contacts (d) and of poles to the lamprophyre contacts (e). Filled circles – second generation of lamprophyres; circles – first generation of lamprophyres, sub-parallel to bedding. The great circles represent the average dip and trend of bedding or of all contacts and the large black square represents the calculated fold axis.

#### **Figure 10**

Large-scale fold mapped in the middle of the deposit showing folding of diorite sills. Note that the bedding is truncated by the diorites suggesting that diorites are just partially sub-parallel to bedding. Also note the preference of mineralization for the hinge zone of the antiform and along diorite-ironstone contacts.

#### **Figure 11**



Wall map showing the relationship between the Geita Hill Shear Zone and the main lithological units in the NE part of the pit along the section C-C' shown in Figure 3. The Geita Hill Shear Zone has an overall sinistral sense of shear. The stereoplots shown at the bottom of the figure illustrate the oblique reverse nature of the GHSZ; b) wall map showing the Geita Hill Shear Zone in the SW part of the deposits (see inset in Figure 3) where it manifests mostly as a series of fracture zones running mostly sub-parallel to bedding. Dashed red lines show fractures without observed displacement; the thick yellow lines mark the extent of the ore zone; c) photograph of an underground exposure of the Geita Hill Shear Zone showing deflection around the diorite body; d) photograph showing the Geita Hill Shear Zone sub-parallel to bedding; e) stereo plot of poles to the shear zone segments that make up the Geita Hill Shear Zone, the great circle shows the average dip and trend of the Geita Hill Shear Zone.

## **Figure 12**

3D cartoon illustrating the general relationship between the Geita Hill deposit ore body, D<sub>3</sub> folded diorite, ironstones and late D<sub>7</sub> faults. Not to scale.

## **Figure 13**

a) Stereo plot showing the poles (black circles) to high grade ore lenses ( $\geq 5\text{g/t}$ ) and the plunge (crosses) of the high grade ore shoots for Geita Hill (GH) deposit; b) stereo plot showing the poles of the high grade ore lenses and the plunge of the ore shoots in the NE part of the Geita Hill gold deposit; c) stereo plot of poles to high grade ore lenses and the plunge of the ore shoots in the SW part of Geita Hill gold deposit; d) stereo plot showing the intersection between the average trend of D<sub>6</sub> Geita Hill Shear Zone and the average trend of D<sub>3</sub> fold axial planes; e) stereo plot showing the intersection between the average trend of

1124 bedding and the average trend of diorites; f) stereo plot showing the intersection between the  
1125 average trend of the Geita Hill Shear Zone and the average trend of bedding; g) stereo plot  
1126 showing the intersection between the average trend of the Geita Hill Shear Zone and the  
1127 average trend of diorites; h) stereo plot showing the location of the intersection (see f, g, h  
1128 and i) of different structural elements (black star – intersection of the average trend of GHSZ  
1129 and the average trend of D<sub>3</sub> folds axial planes; black cross – intersection of the average trend  
1130 of bedding and the average trend of diorite; black square – intersection of the average trend of  
1131 GHSZ and the average trend of bedding; black circle – intersection of the average trend of  
1132 GHSZ and the average trend of diorite).

1133

1134 **Table captions**

1135 **Table 1**

1136 Summary of main deformation and intrusive events recorded in the Geita Hill gold deposit  
1137 and the surrounding area.



**Figure 1**

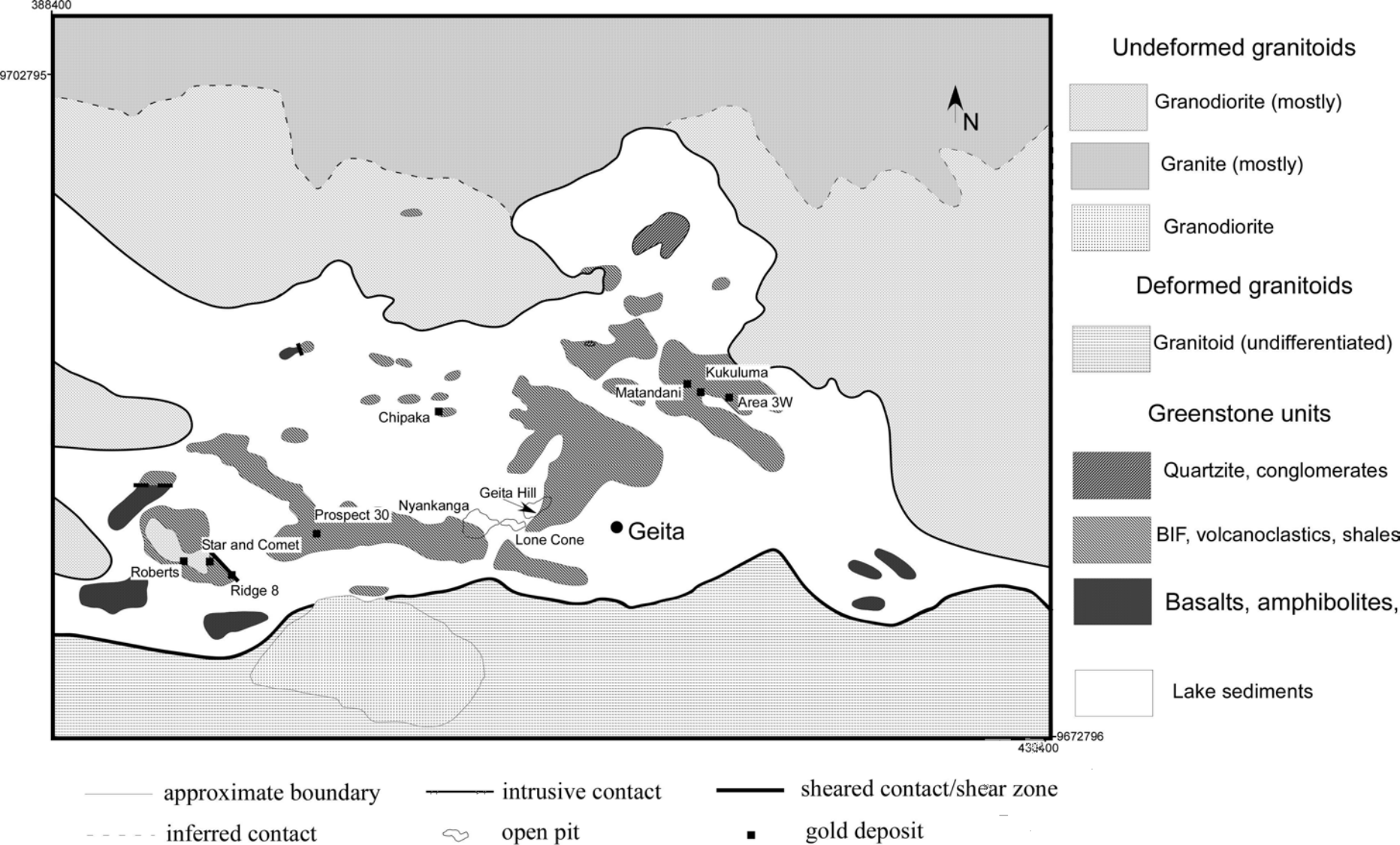
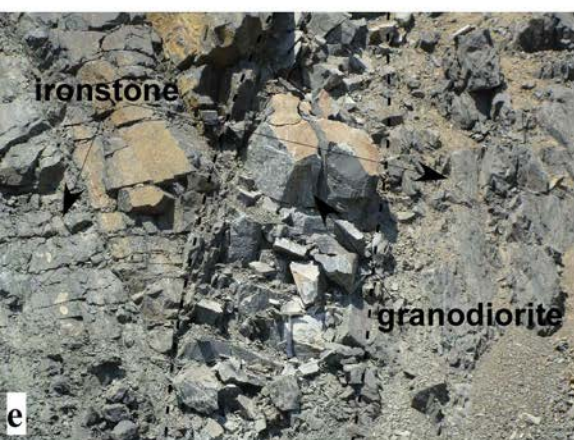
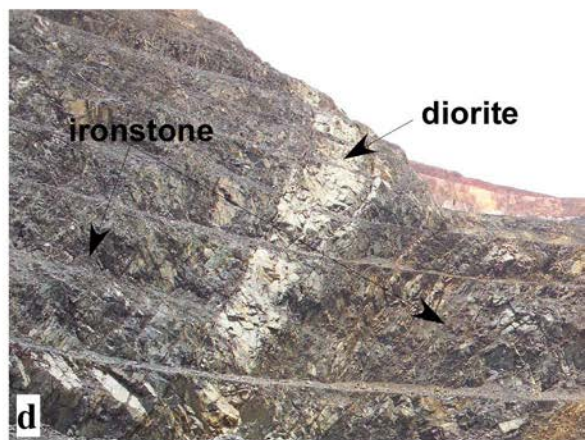


Figure 2



**Figure 3**



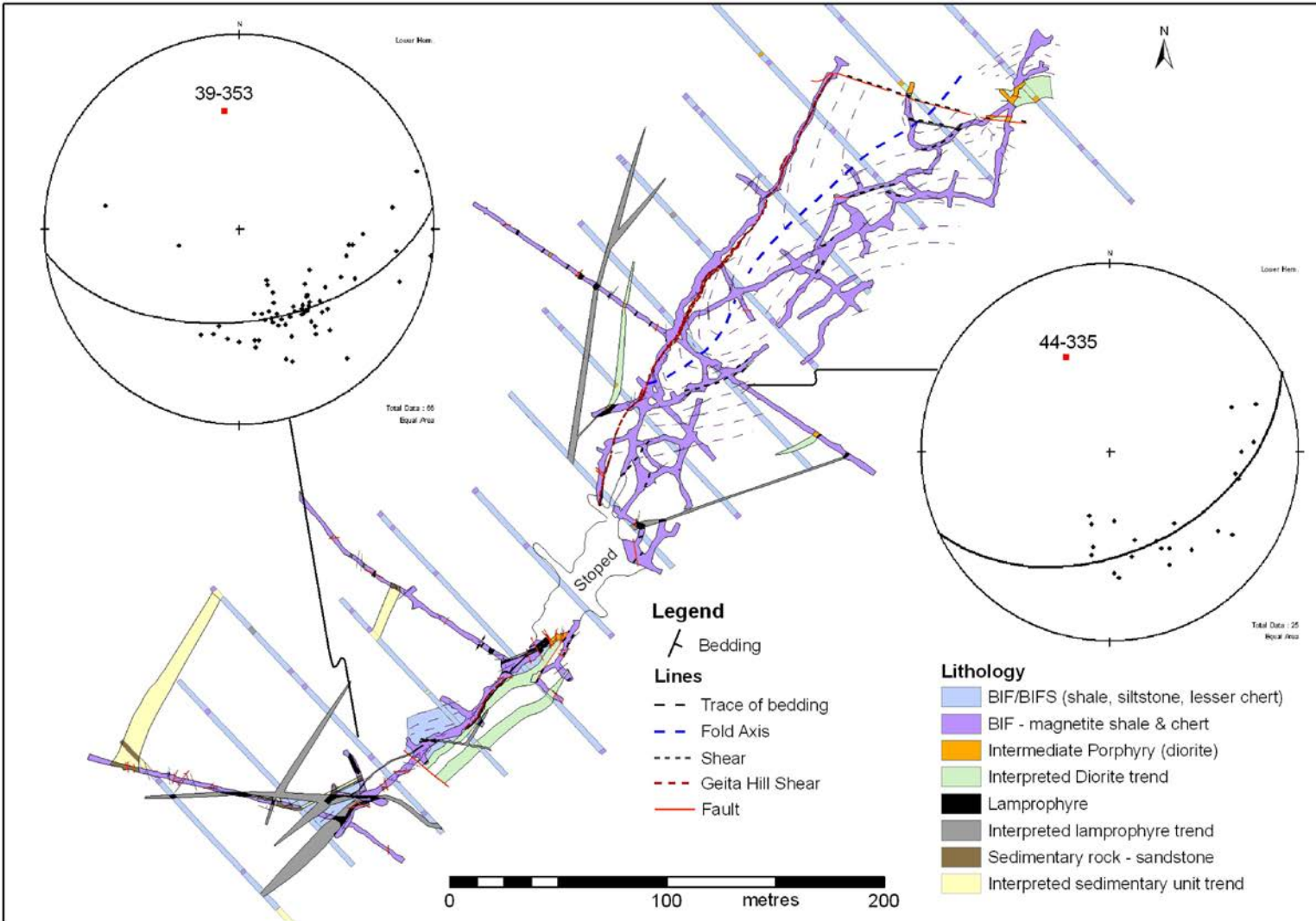


Figure 5



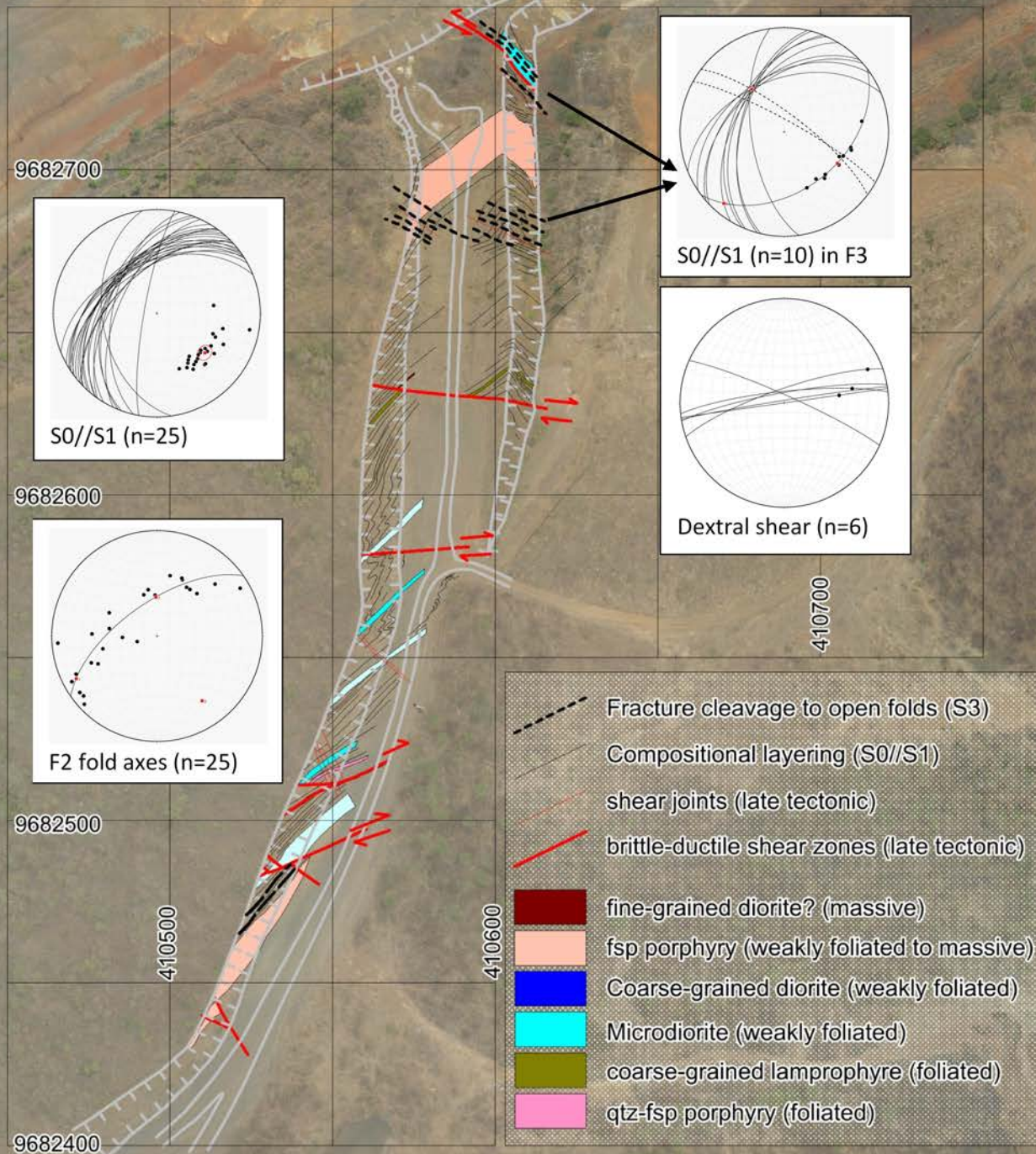
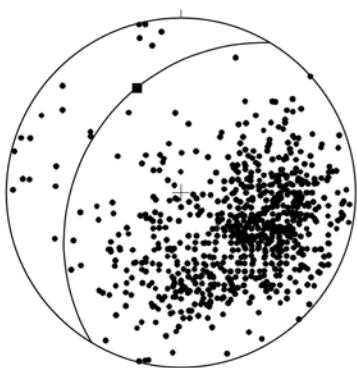




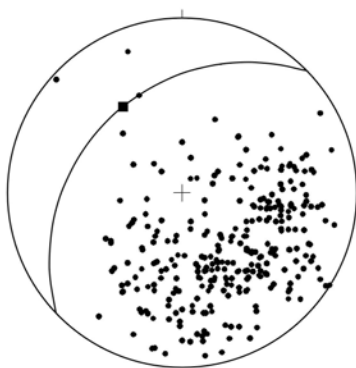


Figure 7

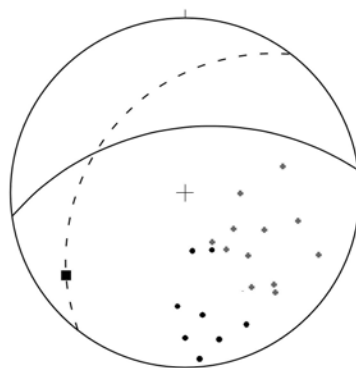




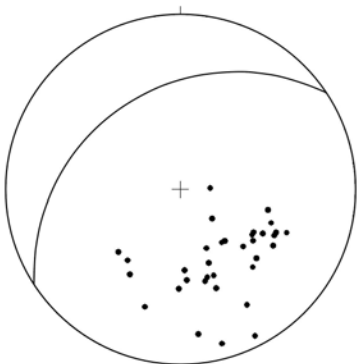
**a)**



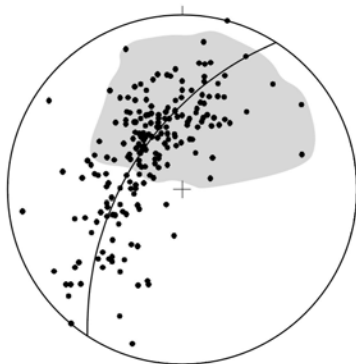
**b)**



**c)**



**d)**



**e)**

**Figure 8**

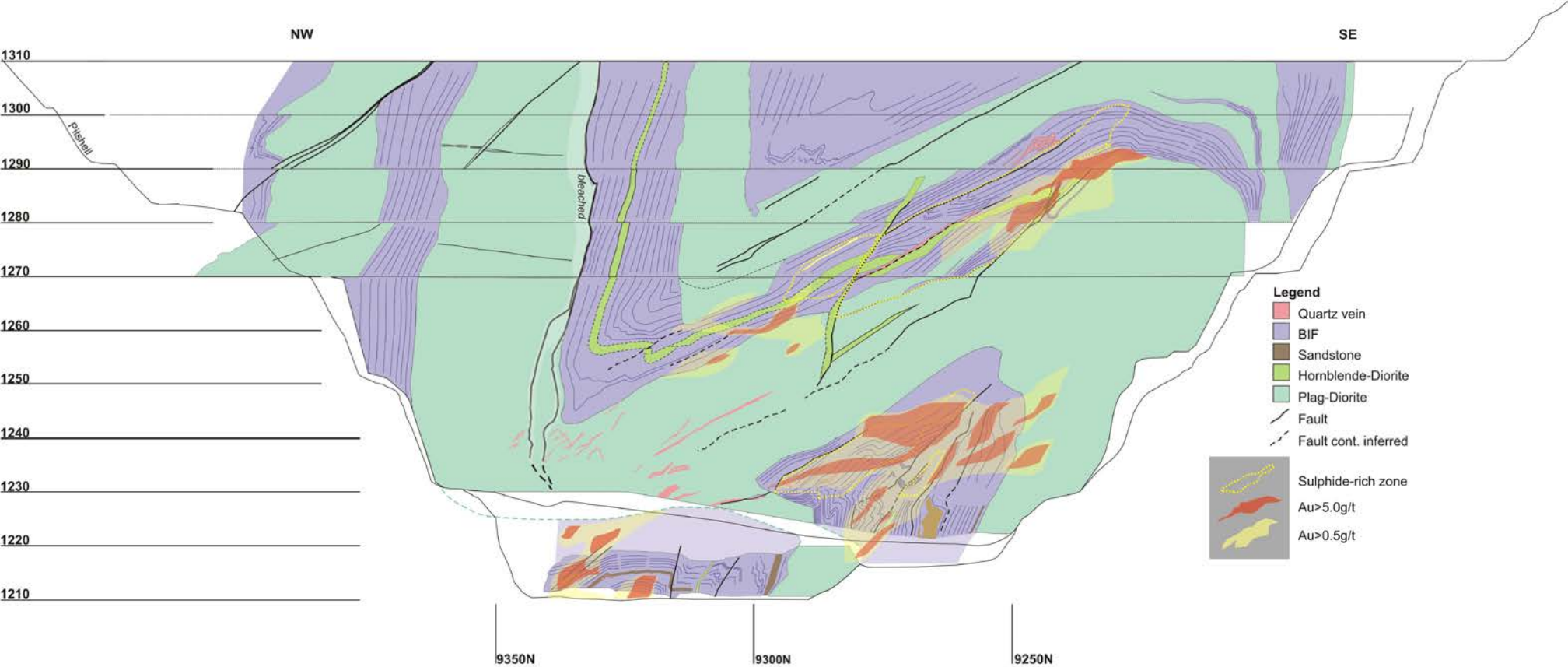
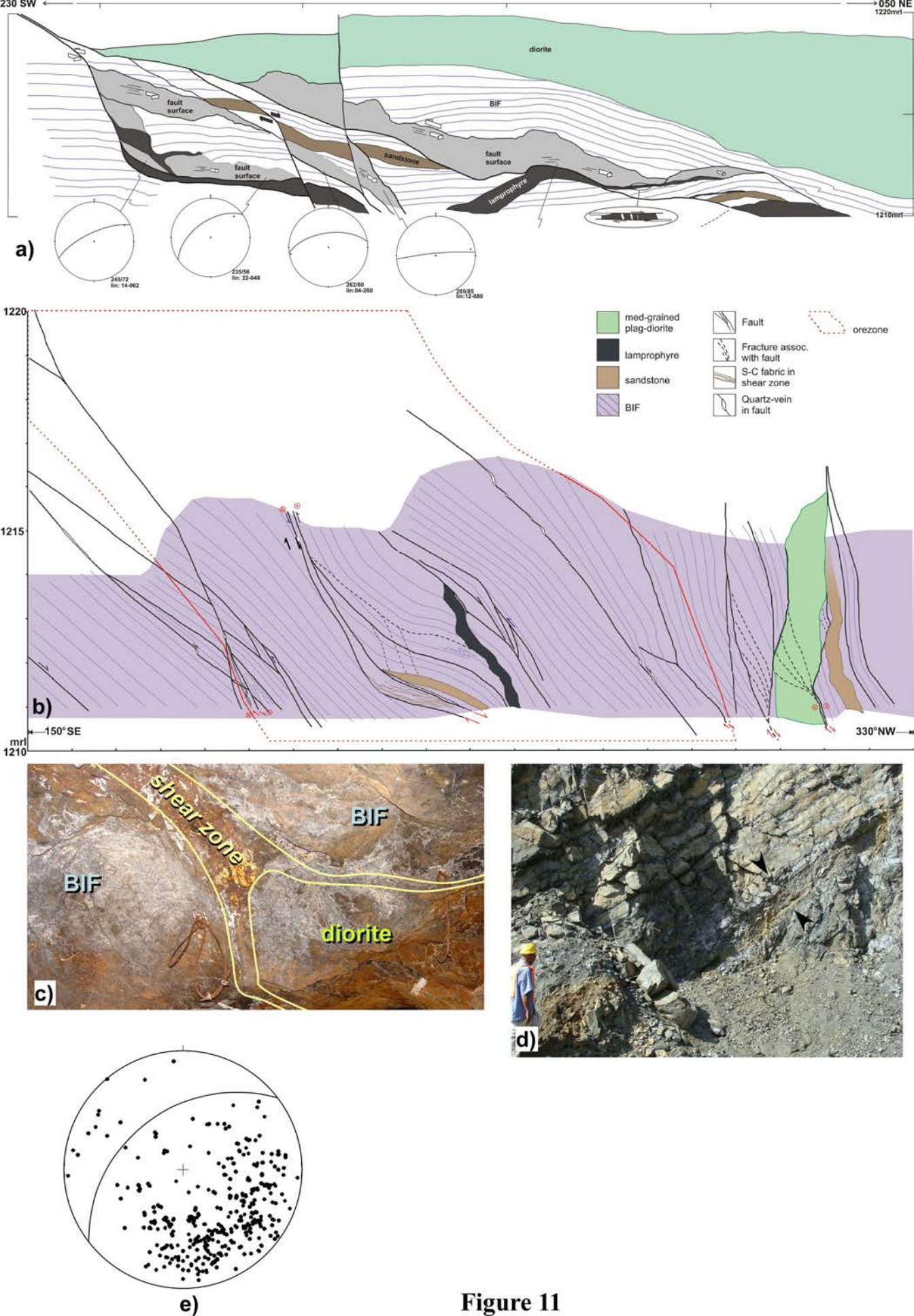
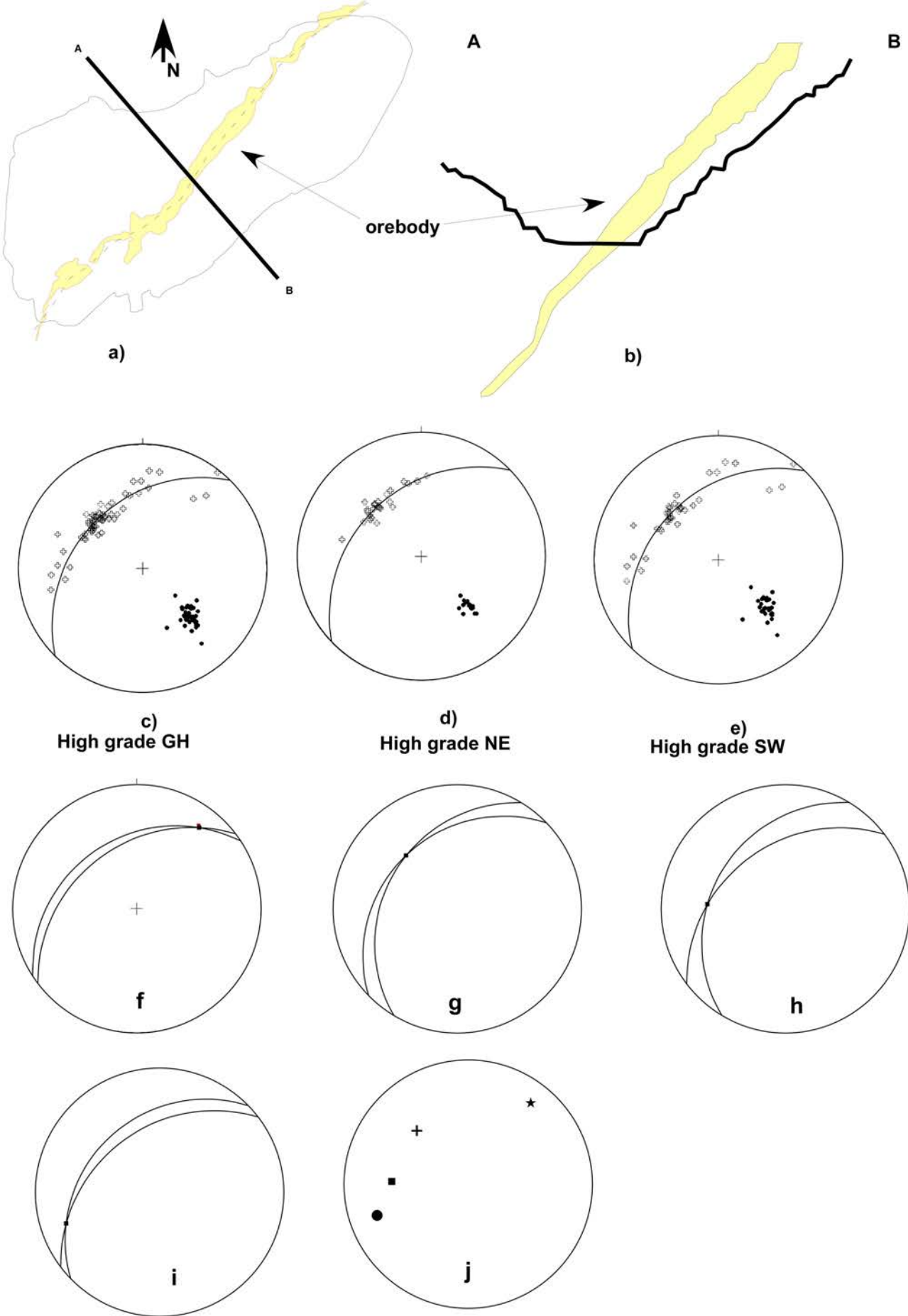


Figure 9



**Figure 11**



**Figure 11**



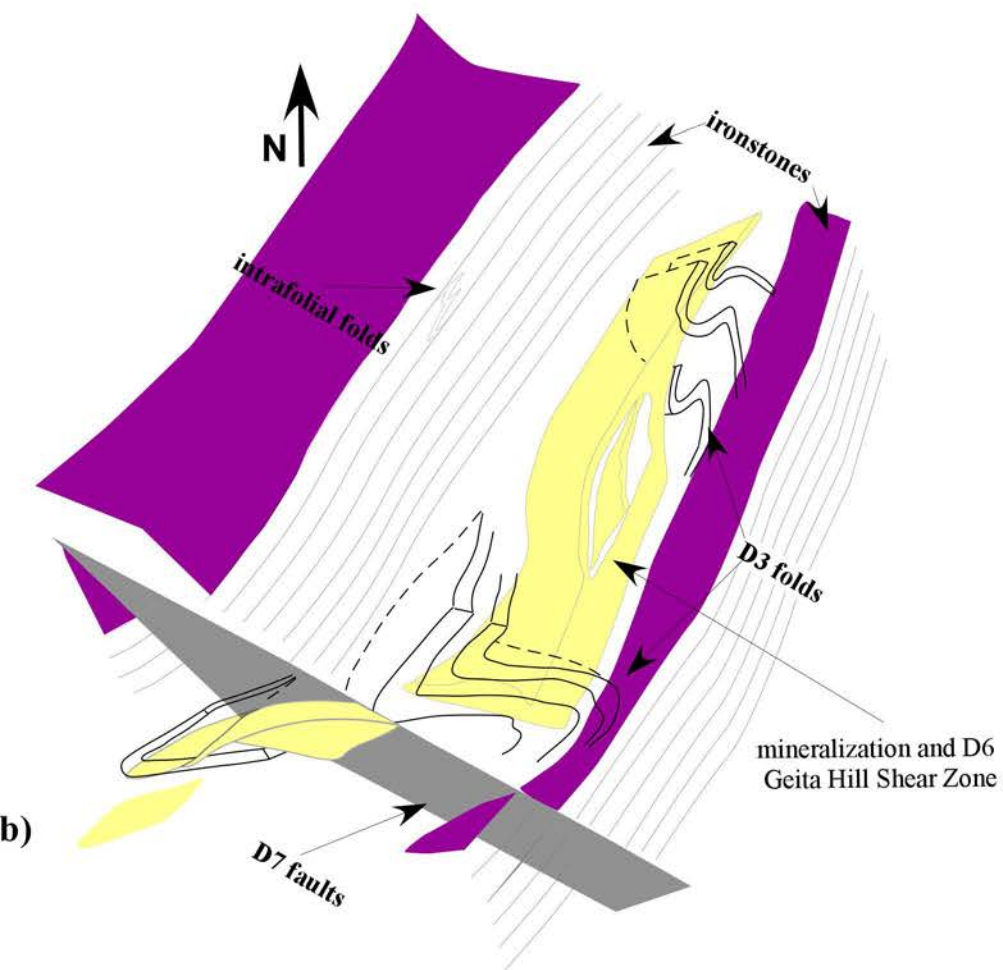
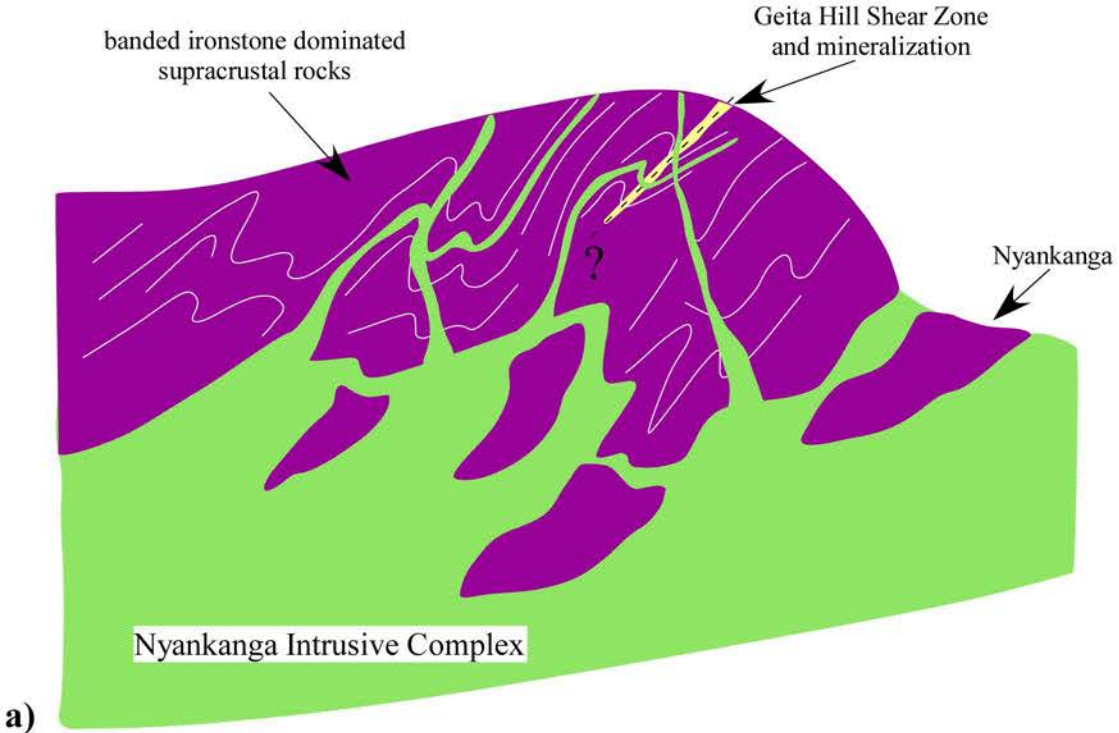


Figure 12